Cooperative Ca^{2+} Removal from Presynaptic Terminals of the Spiny Lobster Neuromuscular Junction

Kiyoshi Ohnuma,* Tomoki Kazawa,* Shunichi Ogawa,* Naoya Suzuki,* Akiko Miwa,# and Hiromasa Kijima*
*Department of Physics, School of Science, Nagoya University, Nagoya 464-8602, and #Department of Neurobiology, Tokyo Metropolitan Institute of Neuroscience, Fuchu 183, Japan

ABSTRACT Stimulation-induced changes in presynaptic free calcium concentration ($[Ca^{2+}]_i$) were examined by fluorescent imaging at the spiny lobster excitor motor nerve terminals. The Ca^{2+} removal process in the terminal was analyzed based on a single compartment model, under the assumption that the Ca^{2+} removal rate from the terminal cytoplasm is proportional to *n*th power of $[Ca^{2+}]_i$. During 100 nerve stimuli at 10–100 Hz, $[Ca^{2+}]_i$ reached a plateau that increased in a less-than-linear way with stimulation frequency, and the power index, *n*, was about 2. In the decay time course after stimulation, *n* changed with the number of stimuli from about 1.4 after 10 stimuli to about 2 after 100 stimuli. With the change of *n* from 1.4 to 2, the rate became larger at high $[Ca^{2+}]_i$ ($>1.5\ \mu M$), but was smaller at low $[Ca^{2+}]_i$ ($<1\ \mu M$). These results suggest that a cooperative Ca^{2+} removal mechanism of $n = 2$, such as mitochondria, may play an important role in the terminal. This view is supported by the gradual increase in the $[Ca^{2+}]_i$ plateau during long-term stimulation at 20–50 Hz for 60 s and by the existence of a very slow $[Ca^{2+}]_i$ recovery process after this stimulation, both of which may be due to accumulation of Ca^{2+} in the organelle.

INTRODUCTION

The intracellular free Ca^{2+} in the presynaptic nerve terminal plays key roles in transmitter exocytosis and in some forms of synaptic plasticities (Dodge and Rahamimoff, 1967; Magleby and Zengel, 1982; Zucker, 1996). Most forms of short-term synaptic plasticity have been shown to be generated by residual presynaptic Ca^{2+} (Katz and Miledi, 1968; Tanabe and Kijima, 1992; Kamiya and Zucker, 1994; Delaney and Tank, 1994; Atluri and Regehr, 1996; Zucker, 1996). However, it is not yet fully understood how the terminal's free Ca^{2+} concentration ($[Ca^{2+}]_i$) is regulated and how this regulation changes during and after tetanic stimulation in presynaptic terminals.

Neuronal Ca^{2+} is regulated by endogenous buffers, extrusion by Ca^{2+} pump and Na^+/Ca^{2+} exchanger through the plasma membrane, uptake into intracellular organelles such as the mitochondria and endoplasmic reticulum, and release from these organelles (Luther, 1992; Hua et al., 1993; Fujii et al., 1996; Tang and Zucker, 1997; Regehr, 1997). These systems have a different dependence on $[Ca^{2+}]_i$. Ca^{2+} pump and Na^+/Ca^{2+} exchanger have a Hill coefficient of about 1, i.e., their rate of Ca^{2+} removal from the terminal cytoplasm is proportional to $[Ca^{2+}]_i$ at low $[Ca^{2+}]_i$ (Carafoli, 1996; Mullins, 1977). However, the mitochondria and endoplasmic reticulum take up Ca^{2+} in a cooperative manner, with a Hill coefficient of about 2 (Bygrave et al., 1971; Scarpa and Graziotti, 1973; Lytton et al., 1992; Gunter et al., 1994). Before we study the contribution of each of the above components to the dynamics of $[Ca^{2+}]_i$, it is important to study quantitatively how the overall $[Ca^{2+}]_i$ is regulated and to analyze it under the assumption that there are some unknown cooperative Ca^{2+} removal mechanisms.

To understand how the Ca^{2+} is regulated, we applied rapid-scanning confocal imaging techniques to the spiny lobster excitor motor nerve terminals loaded with fluorescent Ca^{2+} indicators and measured the nerve stimulation-induced changes in $[Ca^{2+}]_i$ ($[Ca^{2+}]_i$ transients) associated with various tetanic stimulation patterns. The $[Ca^{2+}]_i$ transients during and after stimulation (10–100 stimuli at 10–100 Hz, 60 s stimulation at 4–50 Hz) were analyzed by the single compartment model assuming that the Ca^{2+} removal rate from the terminal cytoplasm is proportional to an *n*th power of $[Ca^{2+}]_i$ change from the resting level ($\Delta[Ca^{2+}]_i^n$). This analysis is useful to gain an insight into the overall features of mixture of several Ca^{2+} removal systems with a minimum number of parameters.

MATERIALS AND METHODS

Preparation

We performed all experiments on the distal accessory flexor muscle (DAFM) of the walking leg of spiny lobsters (*Palinurus japonicus*) weighing about 200 g (cf. Walrond et al., 1993). The DAFM, together with a piece of exoskeleton, a tendon, and an innervating excitatory (glutamatergic) motor axon, was removed from the meropodite as shown in Fig. 1.

To block the movement of the DAFM, we used Joro spider toxin (JSTX-3; Wako, Osaka, Japan), which is a potent antagonist of glutamate receptors of the crustacean muscle and a practically irreversible blocker of excitatory synaptic transmission (Abe et al., 1983; Shudo et al., 1987). The effect of JSTX-3 was use-dependent (Iino et al., 1996), so the excitatory axon was stimulated by 3 stimuli at 20-ms intervals every 3 s for 60 min under a perfusion of spiny lobster physiological saline containing 20 μM JSTX-3, and then washed out.

Dissection and fluorescent image acquisition was performed in spiny lobster physiological saline containing 468 mM NaCl, 10 mM KCl, 20 mM $CaCl_2$, 8 mM $MgCl_2$, and 5 mM HEPES-Na (pH 7.4) (Kawai et al., 1972). All experiments were performed at 17.0 ± 0.5°C.

Received for publication 7 January 1998 and in final form 8 January 1999.
Address reprint requests to Hiromasa Kijima, Ph.D., Department of Physics, School of Science, Nagoya University, Nagoya 464-8602 Japan. Tel.: 81-52-789-2878; Fax: 81-52-789-2879; E-mail: kijima@synapse.phys.nagoya-u.ac.jp.

0006-3495/99/04/1819/16 $2.00

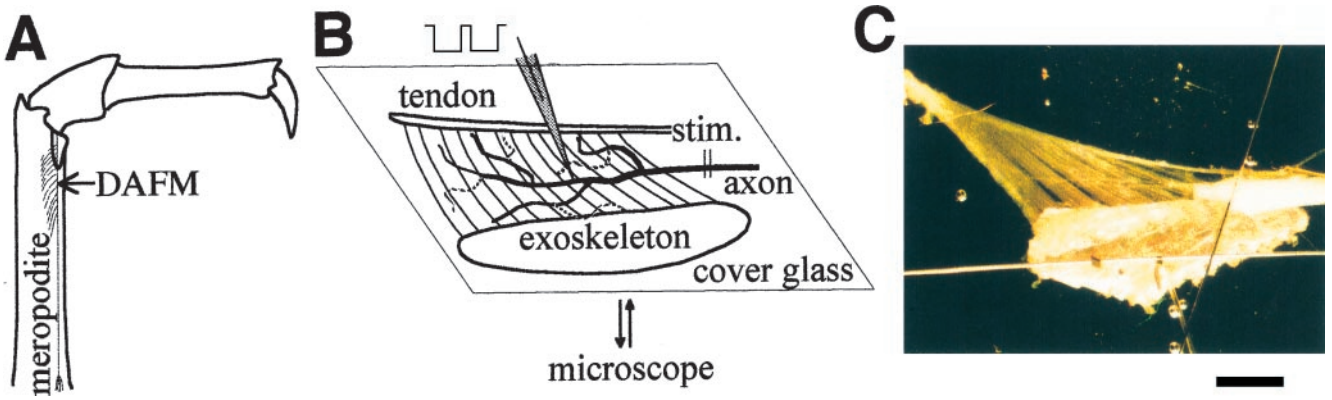

FIGURE 1 Illustration of a preparation. (*A*) Distal accessory flexor muscle (DAFM) in the meropodite of a walking leg of the spiny lobster. The meropodite of spiny lobster weighed about 200 g and measured 30–50 mm in length and 5–10 mm in width. (*B*) Schematic representation of a DAFM preparation and the microelectrode position for dye injection. (*C*) Photograph of DAFM. Stainless steel wire (Nilaco, Tokyo) and fishing line used to fix the preparation are seen. Scale bar: 2 mm.

Injection of fluorescent Ca^{2+} indicator

The excitatory axon, 10–30 μm in diameter, was penetrated near the second branch (Fig. 1 *B*) with a glass microelectrode (15–30 MΩ when filled with 3 M KCl) filled with either 20 mM Oregon Green 488 BAPTA-1 hexapotassium salt (OGB-1; Molecular Probes, Eugene, OR) or Oregon Green 488 BAPTA-2 octapotassium salt (OGB-2) in 200 mM KCl and 10 mM MOPS-KOH (pH 7.3) (Dojindo, Kumamoto, Japan).

OGB-1 or -2 was iontophoresed into the excitatory axon by passing a 1 Hz, 85% duty cycle, 2- to 10-nA hyperpolarizing current pulse for 15–60 min. After waiting 3–5 h for the dye to diffuse, microfluorometric measurements were started. The final concentrations of OGB-2 were estimated to be 100–500 μM in eight normal (not overloaded) terminals by comparing their fluorescence with the fluorescence intensity of a Ca^{2+}-free pseudo-intracellular solution containing the dye (100 or 200 μM) in a glass capillary 1–8 μm in diameter (see in vitro calibration of Ca^{2+} indicator).

Microfluorometric measurement of $[Ca^{2+}]_i$

The preparation was fixed on a cover-glass-bottomed experimental chamber placed on the stage of an inverted microscope TMD-300 (Nikon, Tokyo) so that the fine presynaptic terminals on the surface of the muscle were located a short working distance ($<$200 μm) from an objective (Plan Apo 60$\times$ water, N.A. 1.2; Nikon). Preparations were perfused in the chamber with the spiny lobster physiological saline. Fluorescence images of presynaptic terminals were acquired using a confocal laser-scanning microscope (Odyssey-XL; Noran Instruments, Middletown, WI) attached to the inverted microscope. Fluorescence was excited by the 488-nm line of an argon ion laser, and emission of the Ca^{2+} indicator dye was monitored at a wavelength longer than 515 nm using a dichroic mirror (DM505, Nikon) and a barrier filter (LP515, Odyssey attachment). The confocal slit was 100 μm in width. To estimate the spatial resolution of the system under this condition, we acquired images of fluorescent point sources (fluorescent beads 0.17 μm in diameter: P-7220 component B, Molecular Probes). The half-maximal widths were 0.49 and 0.33 μm on the focal plate (in the *x–y* plane, parallel and perpendicular to the confocal slit, respectively), and 1.10 μm in the *z* axis perpendicular to the focal plane.

The short-term stimulation protocols were 10 and 100 stimuli at 10, 13.3, 20, 33.3, 50, and 100 Hz, and 20 and 50 stimuli at 10, 20, 50, and 100 Hz, respectively. The long-term protocol was stimulation for 60 s at 4, 10, 13.3, 20, 33.3, and 50 Hz. After measurements at 10, 20, 50, and 100 stimuli and stimulation for 60 s, we waited more than 1, 2, 4, 8, and 10 minutes, respectively, for recovery of $[Ca^{2+}]_i$ to the resting level and then measured at another stimulation pattern. The main excitatory axon was stimulated by a pair of Pt-Ir wires with 1–6 V $\times$ 0.1 ms pulses supplied through an isolator from a stimulator.

In the short-term stimulation protocol, fluorescence images were acquired at video rate (30 images/sec; scanning 120 or 240 images/sec, then averaging for 4 or 8 images), usually for a period longer than 25 s, to examine $[Ca^{2+}]_i$ change at a stimulation pattern. For analysis, we used a total period less than 21 s consisting of 1 s before stimulation, stimulation duration, and 10 s after stimulation. Because OGB-1 and -2 had high fluorescence intensity and showed little bleaching, we could reduce laser intensity to 2–5% of its peak without compromising a good signal-to-noise ratio. The fluorescent intensity decreased only slightly, at most a few percent, from before stimulation (resting level) to 25 s after stimulation. When this fluorescence decrease was not negligible, the signal during a period of analysis was compensated for dye bleaching. The fluorescence intensities before stimulation and those for times more than 25 s after the start of image acquisition were fitted with a single exponential curve, and the decrease of intensity from the resting level was added to the observed one. The fluorescence intensities of the terminal region and adjacent background region of each image were spatially averaged and converted into numerical data. For the long-term analyses with stimulation for 60 s, the fluorescence intensities of a rectangular area included in a terminal bouton were acquired as numerical data at video-rate before, during, and after stimulation, for more than 150 s altogether. The fluorescence intensity again decreased only slightly, at most a few percent.

Background signals were subtracted from fluorescence signals (Fig. 2 *A*). Relative fluorescence changes ($\Delta F/F$), where F is fluorescence intensity at the resting state before stimulation and ΔF is the change in fluorescence intensity from F, were converted to $[Ca^{2+}]_i$ values using the following formula (Grynkiewicz et al., 1985; Jaffe et al., 1992):

$$[Ca^{2+}]_i = \frac{[Ca^{2+}]_{rest} + K_B \dfrac{\Delta F/F}{\Delta F_{max}/F}}{1 + \dfrac{\Delta F/F}{\Delta F_{max}/F}} \qquad (1)$$

where K_B is the estimated dissociation constant of OGB-1 or -2 for Ca^{2+}, $\Delta F_{max}/F$ is the maximum $\Delta F/F$ change upon calcium saturation, and $[Ca^{2+}]_{rest}$ is the resting level of $[Ca^{2+}]_i$, which was assumed to be 100 nM.

In vitro calibration of Ca^{2+} indicator

Using a spectrofluorometer (F-4500; Hitachi Ltd., Tokyo), the dissociation constant and $\Delta F_{max}/F$ of these indicators were obtained in vitro from the

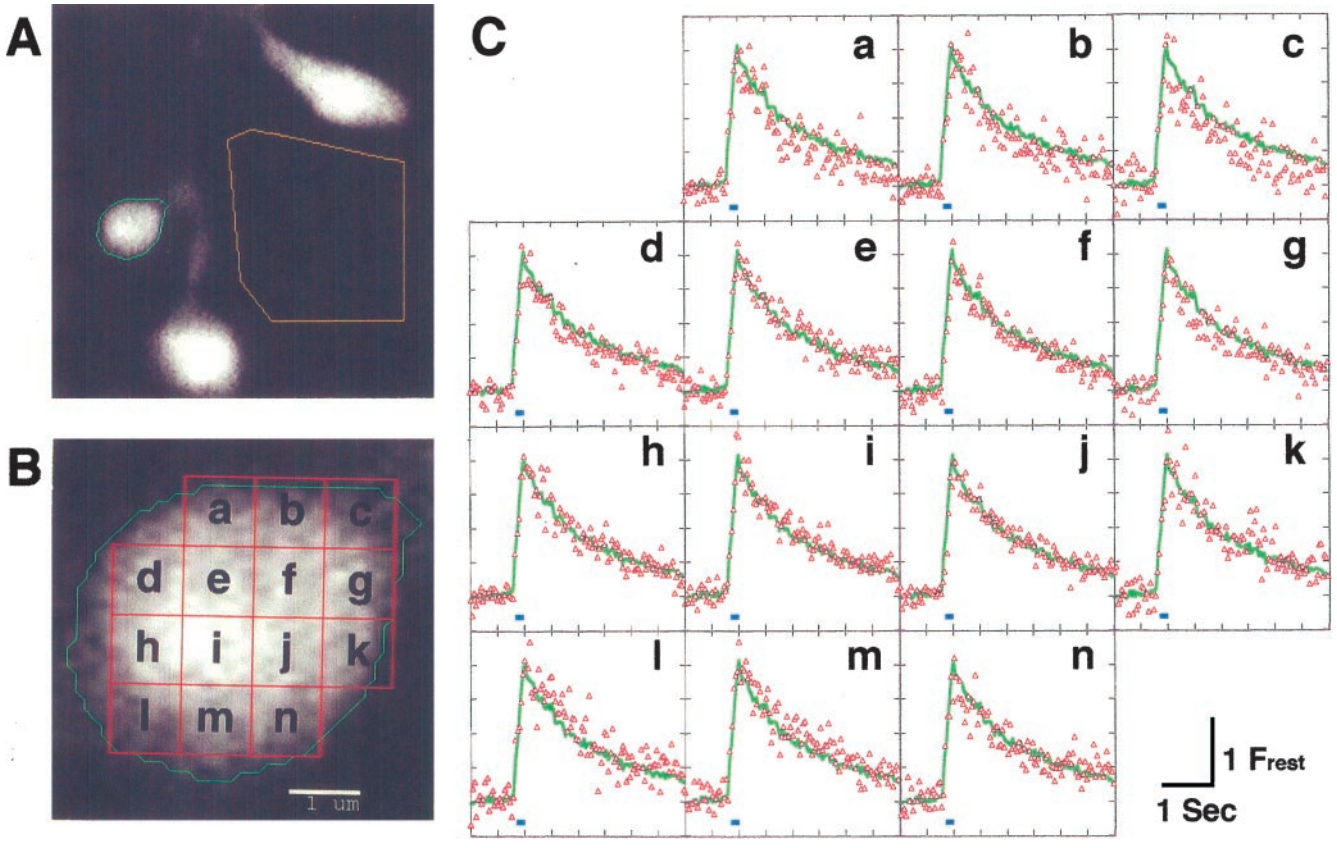

FIGURE 2 Difference between a fluorescence change obtained from the whole nerve terminal and changes obtained from compartmentalized regions during and after short-term stimulation. (*A*) Fluorescence image of presynaptic terminals loaded with OGB-1. There are three spherical or oval shaped presynaptic nerve terminals 4–10 μm in diameter. Intensities in the right region, enclosed with a yellow line, were averaged to estimate the background fluorescence level. (*B*) Higher magnification of middle left nerve terminal in (*A*). A spherical nerve terminal enclosed with a green line in (*A*) and (*B*) designates the whole nerve terminal region; red squares (1×1 μm) show compartmentalized regions (a–n). Scale bar, 1 μm. (*C*) The time-courses of spatially averaged relative fluorescence intensities $\Delta F/F$ of the whole nerve terminal (*green lines*) and of the regions (*red open triangles*) shown in (*B*). Periods of 20 tetanic stimuli at 100 Hz are shown by blue horizontal bars. Increases in $\Delta F/F$ correspond to increases in $[Ca^{2+}]_i$. There were no significant differences in the time-course of the whole nerve terminal and that of each region.

relationship between the OGB-1 or -2 fluorescence and the known concentration of Ca^{2+} in a pseudo-intracellular solution at 17°C. This solution contained 0.5 μM OGB-1 or 0.35 μM OGB-2, 50 mM NaCl, 400 mM KCl, 20 mM MOPS-KOH (pH 7.2), 10 mM EGTA, 10 mM free Mg^{2+}, and various concentrations of $CaCl_2$ with 10 mg/ml bovine serum albumin (A4378, Sigma, St. Louis, MO), which was assumed to mimic endogenous cytoplasmic proteins affecting the Ca^{2+} dependence of indicator fluorescence (Konishi et al., 1988; Baker et al., 1994). K_B and $\Delta F_{max}/F$ of OGB-1 and -2 thus obtained were 0.95 μM and 3.7, and 3.0 μM and 7.2, respectively.

A single compartment model

Formulation

Fluorescence signals of the Ca^{2+} indicators were collected from the whole area of spherical or oval-shaped terminal boutons 4–10 μm in diameter at video rate (30 images/s). Therefore, these signals represent spatio-temporal averages of cytosolic Ca^{2+} signals. In the short-term stimulation protocol, they were analyzed assuming a single compartment model (Neher and Augustine, 1992; Tank et al., 1995; Helmchen et al., 1997). This model assumes instantaneous Ca^{2+} influx and neglects spatial inhomogeneities and outflow from the organelles into the cytoplasmic space. The differential equation for total Ca^{2+} concentration, $[Ca^{2+}]_{Tot}$, is given as

$$\frac{d}{dt}[Ca^{2+}]_{Tot} = -J_{rm} + J_{in} \quad (2)$$

where J_{rm} is the rate of Ca^{2+} removal from the terminal cytoplasmic space and J_{in} is the rate of Ca^{2+} inflow to the terminal cytoplasmic space. This model was shown to be applicable to the presynaptic terminal of spiny lobster neuromuscular junction (NMJ); see Results (Fig. 2).

Here, we make three assumptions in the short-term analysis. The first is that the free calcium concentration $[Ca^{2+}]_i$ is proportional to $[Ca^{2+}]_{Tot}$:

$$[Ca^{2+}]_{Tot} = (1 + \beta)[Ca^{2+}]_i \quad (3)$$

where β is the linearly approximated Ca^{2+} binding ratio of endogenous buffers and exogenously added Ca^{2+} indicator (see Appendix 1). Their Ca^{2+} binding rates are probably fast enough for obtaining accurate averages of terminal $[Ca^{2+}]_i$, when measured at video rate (Regehr and Atluri, 1995). Moreover, $[Ca^{2+}]_i$ was lower than the dissociation constant of Ca^{2+} indicator, OGB-2 (3.0 μM; see Results and Table 1), and probably lower than that of the endogenous buffer throughout the experiments, as was shown in other terminals (Regehr and Atluri, 1995). Thus, the assumption of a constant value of β is reasonable in our experiments, including the long-term stimulation protocol. The second assumption is a constant Ca^{2+}

TABLE 1 Parameters of $\Delta[Ca^{2+}]_i$ decay after short-term stimulation (OGB-2)

Tetanic Stimulation		Power index	Removal rate (at 1 μM)	$F(0)$	Constant term
Frequency	No.	n	k (s^{-1})	$A + C$ (μM)	$C/(A + C)$ (%)
10 Hz	10	1.34 ± 0.03	2.40 ± 0.32	0.39 ± 0.06	1.1 ± 1.0
	100	1.83 ± 0.06	2.30 ± 0.32	0.55 ± 0.07	−0.9 ± 1.0
13 Hz	10	1.35 ± 0.08	2.70 ± 0.70	0.41 ± 0.07	−0.5 ± 1.1
	100	1.83 ± 0.06	2.54 ± 0.42	0.62 ± 0.07	0.6 ± 0.3
20 Hz	10	1.37 ± 0.07	2.71 ± 0.41	0.47 ± 0.09	0.8 ± 0.5
	20	1.55 ± 0.13	3.07 ± 0.74	0.68 ± 0.09	0.8 ± 0.5
	50	1.71 ± 0.06	2.27 ± 0.28	0.77 ± 0.08	1.3 ± 0.5
	100	1.99 ± 0.07	2.75 ± 0.44	0.77 ± 0.07	0.7 ± 0.5
33 Hz	10	1.48 ± 0.07	3.07 ± 0.47	0.59 ± 0.12	0.1 ± 0.5
	100	2.14 ± 0.09	2.67 ± 0.33	1.05 ± 0.10	1.2 ± 0.9
50 Hz	10	1.46 ± 0.09	3.44 ± 0.71	0.68 ± 0.13	1.9 ± 0.9
	20	1.53 ± 0.08	2.63 ± 0.38	0.97 ± 0.13	0.5 ± 0.3
	50	1.90 ± 0.05	2.64 ± 0.35	1.30 ± 0.16	0.6 ± 0.3
	100	2.11 ± 0.08	2.64 ± 0.35	1.24 ± 0.14	1.5 ± 0.9
100 Hz	10	1.53 ± 0.05	3.25 ± 0.52	1.02 ± 0.23	2.2 ± 1.1
	20	1.67 ± 0.05	2.80 ± 0.37	1.46 ± 0.20	1.3 ± 0.6
	50	1.83 ± 0.02	2.60 ± 0.30	2.03 ± 0.29	2.3 ± 0.4
	100	2.10 ± 0.07	2.94 ± 0.37	1.93 ± 0.26	2.9 ± 0.8

Data were obtained using OGB-2 (100–500 μM). Sample number, $N = 8$.
Values are mean ± SE.
The fitting parameters of Eq. 12, $F(t) = \{(n-1)kt + A^{(1-n)}\}^{1/(1-n)} + C$.

inflow at every stimulus during tetanic nerve stimulation,

$$J_{in} = f\delta_{CaT} \tag{4}$$

where f is the stimulation frequency and δ_{CaT} is the total Ca^{2+} inflow induced by a stimulus (see Discussion). The last assumption is that the overall rate of Ca^{2+} removal from the terminal cytoplasm is proportional to the nth power of the change in $[Ca^{2+}]_i$ from the resting level $[Ca^{2+}]_{rest}$.

$$J_{rm} = \gamma(\Delta[Ca^{2+}]_i)^n \tag{5}$$

with

$$\Delta[Ca^{2+}]_i \equiv [Ca^{2+}]_i - [Ca^{2+}]_{rest} \tag{6}$$

where γ is the Ca^{2+} removal rate constant. This is the low concentration limit of nth order Hill's equation for $\Delta[Ca^{2+}]_i$. The Ca^{2+} removal system may include extrusion across the plasma membrane, uptake into intracellular organelles, or binding to cytoplasmic buffers (Sala and Hernández-Cruz, 1990; Neher and Augustine, 1992; Xu et al., 1997). Mitochondria and endoplasmic reticulum take up Ca^{2+} in a cooperative manner with a Hill coefficient of about 2 (Bygrave et al., 1971; Scarpa and Graziotti, 1973; Gunter et al., 1994; Lytton et al., 1992).

Under the three assumptions (Eqs. 3–6), Eq. 2 is given during stimulation as

$$(1+\beta)\frac{d}{dt}(\Delta[Ca^{2+}]_i) = -\gamma(\Delta[Ca^{2+}]_i)^n + f\delta_{CaT} \tag{7A}$$

$$\frac{d}{dt}(\Delta[Ca^{2+}]_i) = -k(\Delta[Ca^{2+}]_i)^n + f\delta_{CaF} \tag{7B}$$

with

$$k \equiv \frac{\gamma}{1+\beta} \quad \text{and} \quad \delta_{CaF} \equiv \frac{\delta_{CaT}}{1+\beta} \tag{8}$$

where k is the apparent removal rate constant of free Ca^{2+} and δ_{CaF} is the free Ca^{2+} increase induced by a stimulus.

Plateau level of $\Delta[Ca^{2+}]_i$ during tetanic stimulation

At the beginning of a tetanic stimulation, the $\Delta[Ca^{2+}]_i$ sharply increases with the rate, $f\,\delta_{CaF}$, because J_{rm} is small. J_{rm} becomes larger with $\Delta[Ca^{2+}]_i$ increase and eventually becomes equal to J_{in}. Thus $\Delta[Ca^{2+}]_i$ reaches a steady-state plateau value. The plateau value, $\Delta[Ca^{2+}]_{pl}$, is obtained by putting $d(\Delta[Ca^{2+}]_i)/dt = 0$ in Eq. 7A as

$$\log(\Delta[Ca^{2+}]_{pl}) = \frac{1}{n}\log\left(\frac{\delta_{CaT}}{\gamma}f\right) \tag{9}$$

The slope of the logarithmic plot of $\Delta[Ca^{2+}]_{pl}$ versus f gives $1/n$. It is worth noticing that for an arbitrary value of n, the plateau is independent of the Ca^{2+} binding ratio of Ca^{2+} buffer, β, and invariable even when β depends on $[Ca^{2+}]_i$, as in the presence of high affinity Ca^{2+} buffer (Tank et al., 1995).

Decay time course of $\Delta[Ca^{2+}]_i$ after tetanic stimulation

After the end of train simulation, Ca^{2+} inflow is terminated ($f\,\delta_{CaF} = 0$) and $[Ca^{2+}]_i$ decays back to the resting level. Eq. 7B is given as

$$\frac{d}{dt}(\Delta[Ca^{2+}]_i) = -k(\Delta[Ca^{2+}]_i)^n \tag{10}$$

This differential equation is solved analytically for any rational number of n as

$$\Delta[Ca^{2+}]_i = \Delta[Ca^{2+}]_{i,0}\exp(-kt) \qquad (n=1) \tag{11A}$$

$$\Delta[Ca^{2+}]_i = \{(n-1)kt + (\Delta[Ca^{2+}]_{i,0})^{1-n}\}^{1/(1-n)} \qquad (n \neq 1) \tag{11B}$$

where $t = 0$ is the time of the last stimulus and $\Delta[Ca^{2+}]_{i,0}$ is $\Delta[Ca^{2+}]_i$ at $t = 0$. Based on Eq. 11B, we fitted $\Delta[Ca^{2+}]_i$ decay with a function,

$$F(t) = \{(n-1)kt + A^{1-n}\}^{1/(1-n)} + C \qquad (n \neq 1) \tag{12}$$

where $A + C$ is the magnitude of $\Delta[Ca^{2+}]_{i,0}$ and C an additional constant term. To obtain best-fit curves, we used each experimental $\Delta[Ca^{2+}]_i$ datum from $t = 0$ to $t = 10$ s. Because we considered the early period of the decay to be important, we weighted the variance of fitting error per second; eight times in 0–1 s, four times in 1–3 s, twice in 3–6 s. The constant term, C, expresses an additional, much slower Ca^{2+} regulation process regarded as a constant value within 10 s, which cannot be described by Eq. 10 in this model. Mathematically, this treatment is equivalent to replacing the solution of Eq. 10 by $(\Delta[Ca^{2+}]_i - C)$, indicating that the removal system begin to work above the level of $[Ca^{2+}]_i = [Ca^{2+}]_{rest} + C$. In the analysis of $\Delta[Ca^{2+}]_i$ change at long-term stimulation (60 s), we will show that this treatment of the slow process is also adequate to describe the biphasic recovery time course after stimulation.

RESULTS

Applicability of the single compartment model

To examine whether the single compartment model (i.e., $[Ca^{2+}]_i$ in the cytoplasmic space of presynaptic terminals is spatially homogeneous) is consistent with the experimental observations, we compared average $\Delta F/F$ of the whole presynaptic terminal with that of each 1×1 μm square compartment during and after 20 stimuli at 100 Hz using OGB-1 (Fig. 2). If inhomogeneity existed in each 1×1 μm region for more than 10 ms, video-rate measurements of fluorescence intensity could detect it, because our confocal laser microscopy system had a spatial resolution of about 0.5×0.4 μm in the x–y plane and 1.1 μm in the z-direction (see Materials and Methods). The result is shown in Fig. 2 *C*. There was no significant difference between the $\Delta F/F$ change of the whole presynaptic terminal and that of each compartment, indicating that terminal $[Ca^{2+}]_i$ spatially averaged in the z-direction showed no appreciable inhomogeneity in the x–y plane, consistent with the assumption of the single compartment model.

A characteristic time scale, Δt, required for the dissipation of $[Ca^{2+}]_i$ inhomogeneity by diffusion is given by (Tank et al., 1995):

$$\Delta t = \frac{(1 + \beta)(radius)^2}{6D} \approx 220 \text{ ms} \qquad (13)$$

for a Ca^{2+} diffusion constant $D = 3 \times 10^2$ $\mu m^2/s$, $\beta = 100$, and radius $= 2$ μm. Thus, this estimation shows that except for about 200 ms during stimulation, $[Ca^{2+}]_i$ may be homogeneous, consistent with the result in Fig. 2. The similarity of $[Ca^{2+}]_i$ rises and peaks in different compartments during stimulation, when $[Ca^{2+}]_i$ may be inhomogeneous, suggests that Ca^{2+} flows in through the membrane facing the postsynaptic muscle fiber below the terminal and that average $[Ca^{2+}]_i$ is accurately measured. Based on these results, we spatially averaged the fluorescence signals from the whole terminal and analyzed them based on a single compartment model as described below.

Plateau level of $\Delta[Ca^{2+}]_i$ during 100 stimuli

Change in $[Ca^{2+}]_i$ was measured using the indicator OGB-2 during a train of 100 stimuli with various frequencies (10, 13.3, 20, 33.3, 50, and 100 Hz) at the same presynaptic terminal (Fig. 3 *A*). There were sharp increases in $\Delta[Ca^{2+}]_i$ as soon as the tetanic nerve stimulation started. The rise continued for 10–20 stimuli, then slowed down. The $\Delta[Ca^{2+}]_i$ reached a quasi-plateau level after 20–50 stimuli at any stimulation frequency, as clearly seen in Fig. 3 *A* (see also Fig. 7). This quasi-plateau level gradually changed with time during long-term stimulation (Fig. 8); thus it is not a plateau in a strict sense. However, we use the term "plateau" hereafter for simplicity. After the end of stimulation, $\Delta[Ca^{2+}]_i$ plunged sharply and then returned slowly to the basal level; $\Delta[Ca^{2+}]_i = 0$. In all 8 terminals loaded with the usual concentration (100–500 μM) of OGB-2, $[Ca^{2+}]_i$ reached a plateau level within 20 to 70 stimuli at all stimulation frequencies, and the number of stimuli required to reach the plateau was almost independent of the stimulation frequency (see also Figs. 7 and 8).

In contrast, the plateau level depended largely on the frequency. The plateau level ($\Delta[Ca^{2+}]_{pl}$) was obtained by

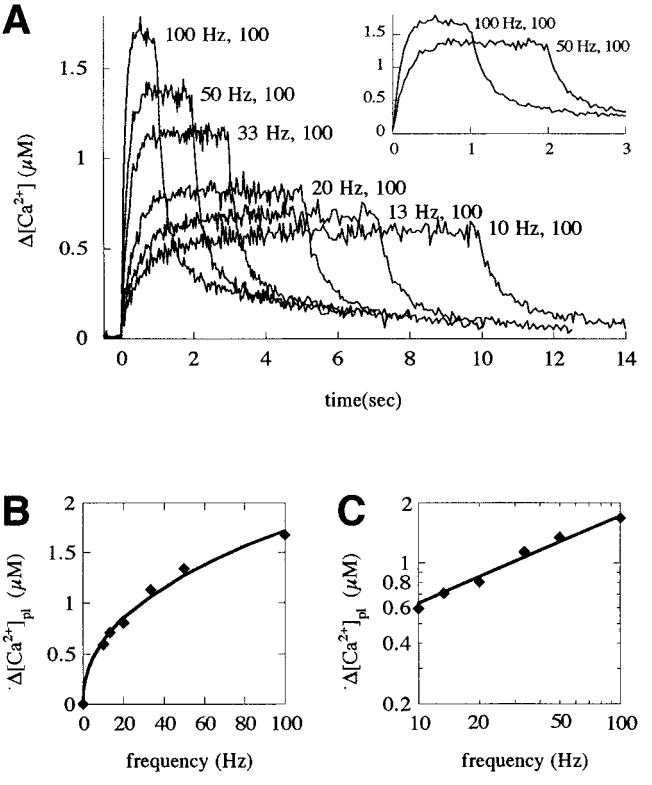

FIGURE 3 Presynaptic changes in $[Ca^{2+}]_i$ during and after the short-term stimulation at a terminal loaded with OGB-2 (not overloaded). (*A*) Time courses of $[Ca^{2+}]_i$ changes from the resting level, $\Delta[Ca^{2+}]_i$, induced by 100 stimuli with various stimulation frequencies (10–100 Hz). The stimulation started at time zero. Inset shows $\Delta[Ca^{2+}]_i$ for 50 and 100 Hz stimulation on an expanded time scale. $\Delta[Ca^{2+}]_i$ reached a plateau after 20–50th stimuli at any stimulation frequency. (*B*) Plateau levels of $\Delta[Ca^{2+}]$ ($\Delta[Ca^{2+}]_{pl}$) shown by closed diamonds, obtained by temporally averaging $\Delta[Ca^{2+}]_i$ during the last 20 (80th to 100th) stimuli, plotted against the stimulation frequency. (*C*) A log-log plot of *B*. The data points were best fitted using Eq. 9, with $n = 2.16$ (2.01 ± 0.10, mean $\pm$ SE, $N = 8$) and $\delta_{CaT}/\gamma = 0.036$ (0.031 ± 0.006, mean $\pm$ SE, $N = 8$). Estimated concentration of OGB-2 was about 200 μM in this terminal.

temporally averaging $\Delta[Ca^{2+}]_i$ during the last 20 (from the 80th to 100th) stimuli. Fig. 3, *B* and *C*, shows $\Delta[Ca^{2+}]_{pl}$ of the example shown in Fig. 3 *A*, plotted against the stimulation frequency. This plot clearly shows a remarkable less-than-linear relationship between $\Delta[Ca^{2+}]_{pl}$ and the stimulation frequency, suggesting a higher Ca^{2+} removal rate at higher $[Ca^{2+}]_i$ (see Discussion). Eq. 9 is the simplest way to analyze this relationship. The power index, *n*, of the fitted curve based on Eq. 9 was 2.16 in Fig. 3, ranging between 1.52 and 2.32, with an average value of 2.01 ± 0.10 (number of samples, $N = 8$), suggesting that the overall Ca^{2+} removal mechanism is highly cooperative. This result is quite different from that of the crayfish NMJ obtained by Tank et al. (1995), which showed complete proportionality between $\Delta[Ca^{2+}]_{pl}$ and stimulation frequency (see Discussion). The value of δ_{CaT}/γ, which shows the ratio of the total Ca^{2+} influx per stimulus (δ_{CaT}) to the Ca^{2+} removal rate constant (γ), was between 0.005 and 0.050, averaging 0.031 ± 0.006. The standard mean error of δ_{CaT}/γ was large, suggesting that δ_{CaT} and γ of each presynaptic terminal are largely variable.

The value of *n* determined from the plots of $\Delta[Ca^{2+}]_{pl}$ against the stimulation frequency was little affected by the kinds of Ca^{2+} indicators and their concentration. In 4 terminals loaded with OGB-1, $n = 2.26 \pm 0.07$ and $\delta_{CaT}/\gamma = 0.012 \pm 0.028$. In 3 terminals overloaded with OGB-2 (1–2 mM), $[Ca^{2+}]_i$ increased more slowly, reached a plateau level after 70–100 stimuli, and returned to the basal level very slowly. In these terminals with the large Ca^{2+} binding ratio β, $n = 2.16 \pm 0.10$ and $\delta_{CaT}/\gamma = 0.069 \pm 0.028$. The values of δ_{CaT}/γ at OGB-1-loaded and OGB-2-overloaded terminals appeared different from those of usual OGB-2-loaded (not overloaded) terminals, but their difference were not statistically significant ($p > 0.05$ by *t* test). As mentioned in Methods, the values of $\Delta[Ca^{2+}]_{pl}$ and *n* should be independent of the magnitude and properties of β, and dependent only on the Ca^{2+} removal mechanism. This was true for the terminals loaded with OGB-1 and those overloaded with OGB-2 (larger β).

The above results indicate that the Ca^{2+} removal rate of the spiny lobster motor nerve terminal behaves as though it were cooperatively dependent on $[Ca^{2+}]_i$ and nearly proportional to a square of $\Delta[Ca^{2+}]_i$, under the assumption of constant Ca^{2+} inflow per stimulus (δ_{CaT}) (second assumption). If this assumption does not hold, i.e., if δ_{CaT} decreases with stimulation frequency due to, for example, an inactivation of Ca^{2+} channels at higher frequency stimulation (higher $[Ca^{2+}]_i$) (cf. Galli et al., 1994), the curve of $\Delta[Ca^{2+}]_{pl}$ versus stimulation frequency (Fig. 3 *B*) becomes less than linear and the power index *n* might become larger than 1. Although it is difficult to prove that this is not the case, the decrease in δ_{CaT} during short-term stimulation is considered to be small (see Discussion).

Decay time course of $\Delta[Ca^{2+}]_i$ after 100 stimuli

Another way to examine the properties of the Ca^{2+} removal mechanism is to study the decay time course of $\Delta[Ca^{2+}]_i$ after the end of short-term stimulation. This decay process depends not on δ_{CaT}, but on the nature of the Ca^{2+} binding ratio, β, as well as the properties of the Ca^{2+} removal mechanism. We analyzed decay of $\Delta[Ca^{2+}]_i$ based on Eq. 12 after 100 tetanic stimuli with various frequencies at the same presynaptic terminal, under the assumption that the β value is a constant (third assumption). This assumption may have been valid when OGB-2 ($K_B = 3.0$ μM) was used as the Ca^{2+} indicator, because the observed $[Ca^{2+}]_i$ was <2 μM. Fig. 4, *A* and *B*, shows an example of a part of a series of measured $\Delta[Ca^{2+}]_i$ at the same synapse loaded with OGB-2, best-fit curves, $F(t)$ (Eq. 12), and the difference between them. These two curves fitted well with almost the same value of *n* (2.06 and 2.07 in this case) and there was no systematic error. Table 1 (OGB-2, $N = 8$) shows that the average value of *n* was about 2 after 100 stimuli at all stimulation frequencies. Even when we used a high affinity Ca^{2+} indicator, OGB-1 ($K_B = 0.95$ μM), the value of *n* was also about 2 after 100 stimuli, as given in Table 2 ($N = 4$). In the OGB-2-overloaded terminals described earlier, *n* was nearly the same (2.03 ± 0.09 at 100 Hz 100 stimuli, $N = 3$) as in the terminals not overloaded, although the free calcium removal rates, *k* (1.22 ± 0.27 at 100 Hz 100 stimuli, $N = 3$), were about half those of the not-overloaded terminal. This

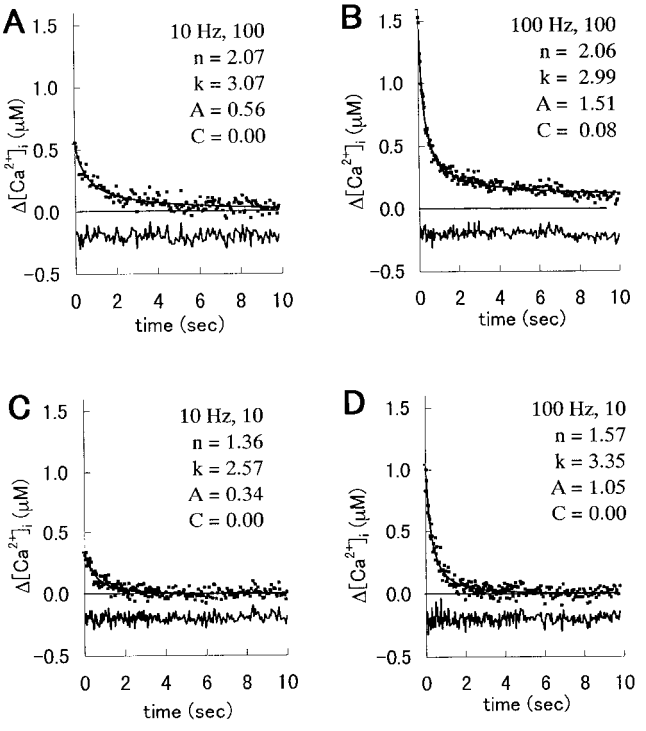

FIGURE 4 Decay time courses of $\Delta[Ca^{2+}]_i$ after short-term stimulation. The examples of decay time course of $[Ca^{2+}]_i$ (*closed squares*) shown were measured at a nerve terminal loaded with OGB-2 after 100 stimuli at 10 Hz (*A*) and 100 Hz (*B*), and 10 stimuli at 10 Hz (*C*) and 100 Hz (*D*). Also shown are best-fit curves (*solid line*) based on Eq. 12 and plots of differences between the data and the fitted lines (solid lines of lower traces, which were shifted by −0.2 μM). The time $t = 0$ is the time of the last stimulus. Values of parameters in Eq. 12 are also shown. Concentration of OGB-2 was estimated to be about 120 μM (not overloaded).

TABLE 2 Parameters of $\Delta[Ca^{2+}]_i$ decay after short-term stimulation (OGB-1)

Tetanic Stimulation		Power index	Removal rate (at 1 μM)	$F(0)$	Constant term
Frequency	No.	n	k (s^{-1})	$A + C$ (μM)	$C/(A + C)$ (%)
20 Hz	10	1.47 ± 0.07	4.84 ± 0.94	0.54 ± 0.06	2.5 ± 1.0
	20	1.62 ± 0.12	4.75 ± 0.85	0.64 ± 0.05	2.3 ± 0.5
	50	1.82 ± 0.07	4.63 ± 0.60	0.66 ± 0.05	3.6 ± 0.8
	100	2.17 ± 0.08	8.53 ± 2.13	0.58 ± 0.06	0.9 ± 1.2
50 Hz	10	1.48 ± 0.06	4.61 ± 0.38	0.64 ± 0.06	2.3 ± 0.6
	20	1.69 ± 0.07	4.29 ± 0.53	0.88 ± 0.09	1.5 ± 0.4
	50	1.88 ± 0.09	4.91 ± 0.96	0.98 ± 0.14	2.6 ± 0.5
	100	2.06 ± 0.09	6.84 ± 2.36	0.94 ± 0.13	3.8 ± 0.5
100 Hz	10	1.47 ± 0.06	4.77 ± 0.59	0.72 ± 0.10	1.9 ± 0.4
	20	1.62 ± 0.01	4.46 ± 0.66	1.00 ± 0.18	2.4 ± 0.3
	50	1.89 ± 0.14	5.92 ± 2.22	1.26 ± 0.32	2.8 ± 0.5
	100	2.14 ± 0.12	6.27 ± 1.54	1.15 ± 0.16	5.0 ± 1.8

Data were obtained using OGB-1. Sample number, $N = 4$.
Values are mean ± SE.
The fitting parameters of Eq. 12, $F(t) = \{(n - 1)kt + A^{(1-n)}\}^{1/(1-n)} + C$.

result is consistent with the prediction of the model that the increasing calcium binding ratio, β, by loading more exogenous Ca^{2+} indicator, does not affect the power index, n, but makes k smaller (Eq. 8).

These results agreed well with that of the plateau level analysis, although the processes depended on different properties of Ca^{2+} dynamics. This suggests the existence of true cooperative Ca^{2+} removal mechanisms at the presynaptic terminals of spiny lobster.

Change in apparent cooperativity of Ca^{2+} decay dependent on number of short-term stimuli

We also analyzed decay of $\Delta[Ca^{2+}]_i$ based on Eq. 12 after 10, 20, and 50 tetanic stimuli with various frequencies at the same presynaptic terminal, using OGB-2 ($N = 8$). The results showed that the values of n changed depending on the number of stimuli. An example is shown in Fig. 4. The value of n was about 1.4–1.6 at 10 stimuli (Fig. 4, *C* and *D*), became larger as the number of stimuli increased, and was close to 2 at 100 stimuli (Fig. 4, *A* and *B*). This change in n occurred in almost the same manner irrespective of the stimulation frequency, as shown in Table 1 (OGB-2). We also analyzed decay of $\Delta[Ca^{2+}]_i$ using OGB-1. Table 2 shows the results. The value of n changed just as in the results obtained by OGB-2 (Table 1). In a recent study at presynaptic terminals of cerebellar parallel fibers, Ca^{2+} decay time courses were also reported to change with the number of stimulation pulses (Regehr, 1997; see Discussion). This change in n may appear to contradict the definite value of n (about 2) obtained by the analysis of the relationship between plateau $\Delta[Ca^{2+}]_i$ and stimulation frequency, but this is not the case. The change in n occurred mostly before the plateau was reached, i.e., after 10 to 20 stimuli. After $\Delta[Ca^{2+}]_i$ had reached nearly the plateau level after 50 and 100 stimuli, the value of n changed only slightly (Table 1 and Fig. 5 *A*).

In Fig. 5 *A*, average values of n and k at all stimulation frequencies, obtained using OGB-2, are plotted against the number of stimuli. The result, that n increased with the number of stimuli, suggests that the tetanic stimulation changed the cooperativity of the Ca^{2+} removal system at presynaptic terminals. Furthermore, this apparent cooperativity was almost independent of the peak $\Delta[Ca^{2+}]_i$, which was nearly equal to $F(0)$ ($= A + C$) in Table 1. This is obvious when we compare the results of 10 and 100 stimuli at 10 and 100 Hz. When the peak $\Delta[Ca^{2+}]_i$ and n at four stimulation patterns were arranged as in Fig. 5 *B*, the peak $\Delta[Ca^{2+}]_i$ became larger from left to right but n depended mostly on the number of stimuli. In contrast to n, the apparent Ca^{2+} removal rate constant, k, which represents the Ca^{2+} removal rate at $\Delta[Ca^{2+}]_i = 1$ μM, was almost independent of both the number and frequency of stimuli (Fig. 5 *A*, Table 1).

It is also worth noticing that C values (or its proportion, $C/(A + C)$, in Table 1) were nearly zero at most stimulation patterns except for 50 and 100 stimuli at 100 Hz. This indicates that the time courses were well described with the model represented by Eq. 10. In 50 and 100 trains at 100 Hz, however, C occupied 2–4% of the total $\Delta[Ca^{2+}]_i$. This indicates that there are contributions of an additional, much slower process that cannot be described by Eq. 10. This slower process may be caused by accumulation of Ca^{2+}, as will be suggested in the analysis of $[Ca^{2+}]_i$ changes due to long-term stimulation below.

Reconstruction of relationship between Ca^{2+} removal rate and $\Delta[Ca^{2+}]_i$ after short-term stimulation

To clarify how the Ca^{2+} removal rate changes with the number of tetanic stimuli, we reconstructed Ca^{2+} removal rates from the results of the decay time course analysis. Using the mean values of n, k, and C given in Table 1

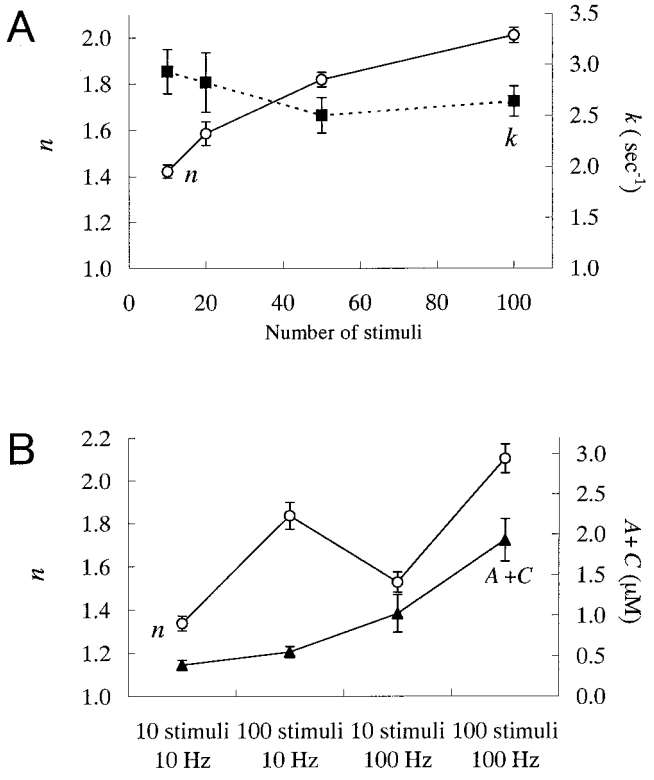

FIGURE 5 Dependence of $[Ca^{2+}]_i$ decay parameters on the number of stimuli after short-term stimuli. (*A*) The power index, *n* (*open circles*, *left ordinate*), and the value of *k*, which represents the free Ca^{2+} removal rate at $\Delta[Ca^{2+}]_i = 1$ μM (*closed rectangles*, *right ordinate*), obtained by averaging these values at all stimulation frequencies given in Table 1 (OGB-2, $N = 8$), were plotted against the number of stimuli (10, 20, 50, and 100 stimuli). (*B*) The power index, *n* (*open circles*, *left ordinate*), and the peak calcium concentration, $A + C$ or $F(0)$ (cf. Eq. 12; *closed triangles*, *right ordinate*), at 10 and 100 stimuli at 10 and 100 Hz in Table 1 (OGB-2, $N = 8$). The index, *n*, depended on the number of stimuli, but depended slightly on the peak $\Delta[Ca^{2+}]_i$. Concentrations of OGB-2 were estimated to be 100–500 μM in these terminals (not overloaded).

(OGB-2), the time courses of Ca^{2+} removal after 10 and 100 stimuli at 100 Hz were reconstructed (Fig. 6 *A*). It is obvious that after 100 stimuli, $[Ca^{2+}]_i$ decayed rapidly first and then became slower, and a higher $[Ca^{2+}]_i$ remained for a long time. Conversely, after 10 stimuli the decay was moderate at first, but rapidly approached the resting level (see also Fig. 4).

Fig. 6, *B* and *C*, shows the relationship between the Ca^{2+} removal rate ($-d(\Delta[Ca^{2+}]_i)/dt$) and $\Delta[Ca^{2+}]_i$. Although we used Eq. 12 containing a constant value *C* that represents deviation from the model, these curves were quite consistent with the differential equation (Eq. 10) of the model, i.e., the log-log plots of the curves in Fig. 6 *C* were almost linear, because the values of *C* were small (<4% of total Ca^{2+} change) (Table 1).

For $\Delta[Ca^{2+}]_i$ values <1 μM, the removal rate was larger after 10 stimuli than after 100 stimuli. In contrast, at $\Delta[Ca^{2+}]_i$ >1.5 μM, the rate was larger after 100 stimuli. The same results were obtained at all stimulation frequencies, indicating that the Ca^{2+} removal mechanism changes from a higher rate at low $[Ca^{2+}]_i$ type to a higher rate at high $[Ca^{2+}]_i$ type with the increase in stimulus number.

Time course of $\Delta[Ca^{2+}]_i$ increase during 100 stimuli

The changes in $\Delta[Ca^{2+}]_i$ decay time course with the number of stimuli shown above suggest that after the start of stimulation, $\Delta[Ca^{2+}]_i$ might deviate from the numerically calculated solution of Eq. 7B, using the parameters, *k* and *n*, determined by analysis of the Ca^{2+} decay time course after 100 stimuli. Fig. 7 shows an example of these differences obtained from an OGB-2-loaded terminal. Because Eq. 7B cannot be solved analytically at a rational number of *n*, we numerically calculated the time-course of $\Delta[Ca^{2+}]_i$ increases by computer. The value of δ_{CaF} is determined so as to fit the calculated plateau level to the measured level.

At the start of stimulation, the observed rates of $\Delta[Ca^{2+}]_i$ increase coincided well with those of the simulated curves in Fig. 7, *A*, *B*, and *C*, because the rate of Ca^{2+} removal is small and contributes little to the initial increase rate of $[Ca^{2+}]_i$.

At low stimulation frequencies (10 and 33.3 Hz; Fig. 7 *A* and *B*), where $\Delta[Ca^{2+}]_i$ is <1 μM throughout the time course, the observed time course is much slower than the time course simulated by calculation. This is expected because the Ca^{2+} removal was more efficient at $\Delta[Ca^{2+}]_i$ lower than 1 μM when the nerve was stimulated fewer times (10 and 20 stimuli before reaching the plateau).

In contrast to this, at 100 Hz stimulation (Fig. 7 *C*), $\Delta[Ca^{2+}]_i$ increased above 1 μM. At these high $\Delta[Ca^{2+}]_i$, the Ca^{2+} removal rate at the small number of stimuli, i.e., in the rising phase of $\Delta[Ca^{2+}]_i$, was lower than that after 100 stimuli. Thus, the observed rate of $[Ca^{2+}]_i$ increase became slightly higher at $\Delta[Ca^{2+}]_i$ near the plateau than on the curve of calculation.

Changes in $[Ca^{2+}]_i$ during long-term stimulation for 60 s

To elucidate further possible contributions of intracellular organelles to Ca^{2+} dynamics and to compare precisely the results obtained here with those of the crayfish NMJ (Tank et al., 1995), we applied long-term stimulation for 60 s at various stimulation frequencies and measured $[Ca^{2+}]_i$ changes using OGB-2. An example of the result is shown in Fig. 8.

The changes in $[Ca^{2+}]_i$ were clearly biphasic. $[Ca^{2+}]_i$ sharply increased at the beginning of stimulation (the early phase) and attained the plateau level after 20–70 stimuli (Fig. 8 *B*, left) in the same way as shown in the short-term stimulation (Fig. 3). After about 100 stimuli it gradually increased during stimulation at frequencies above 20 Hz, but remained almost constant at the stimulation frequency below 13 Hz. The late phase of $[Ca^{2+}]_i$ increase after 100 stimuli was more evident at higher stimulation frequencies.

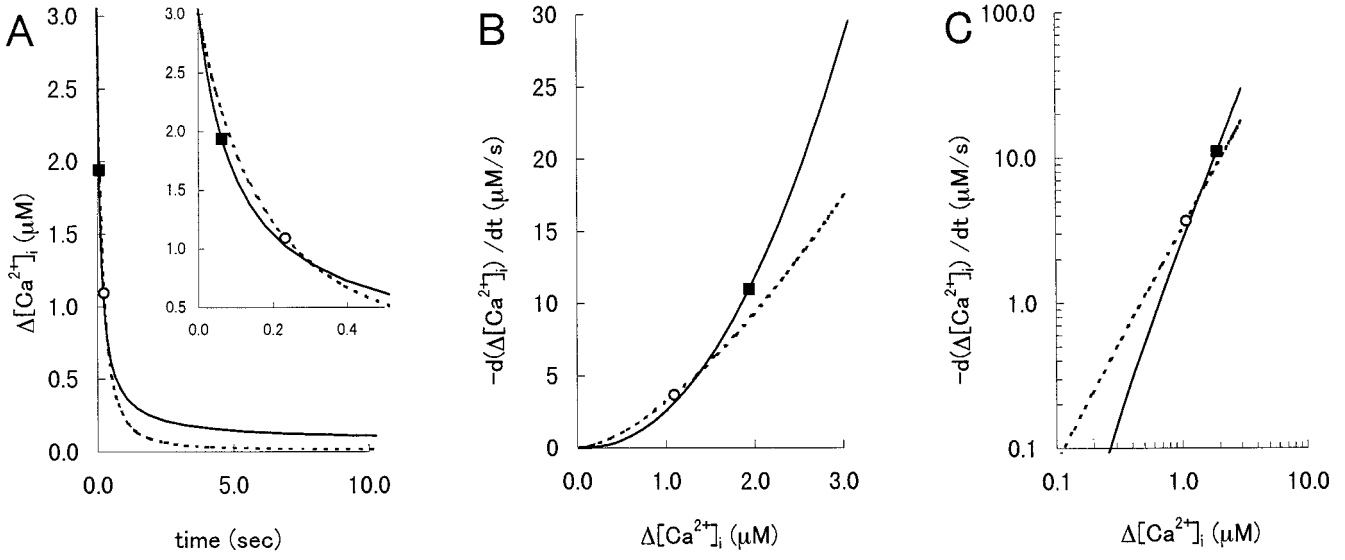

FIGURE 6 Reconstructed $\Delta[Ca^{2+}]_i$ decay and its rate after short-term stimuli. (*A*) Reconstructed $\Delta[Ca^{2+}]_i$ decay time courses after 10 (*dotted curve*) and 100 stimuli (*solid curve*) at 100 Hz stimulation frequencies, using the average values of *n*, *k*, and $C/(A + C)$ obtained from eight OGB-2-loaded terminals (Table 1). Initial concentration, $\Delta[Ca^{2+}]_{i,0}$, is extrapolated to 3 μM by adjusting time 0. Values of $A + C$ for 10 stimuli (*open circle*) and 100 stimuli (*closed rectangle*), which represent peak values, are also shown. Inset shows the initial decay on an expanded time scale. (*B*) and (*C*) The relationship between $\Delta[Ca^{2+}]_i$ and its removal rate, or minus value of the time derivative ($-d(\Delta[Ca^{2+}]_i)/dt$) in (*A*), is shown by a linear plot (*B*) and a log-log plot (*C*).

Because the rate of $[Ca^{2+}]_i$ increase in the late phase was more than 20 times slower than that of the early phase, it is reasonable to think that $[Ca^{2+}]_i$ attained the plateau level within 100 stimuli. When stimulated at 100 Hz, the late phase increase in the $[Ca^{2+}]_i$ became even more evident, but $[Ca^{2+}]_i$ dropped sharply several times for a few seconds during stimulation, probably due to failure of action potential invasion of the terminals. This indicates that $[Ca^{2+}]_i$ change evoked by 100 Hz stimuli is inadequate for quantitative analysis. Three possibilities or combinations of them may account for this late phase increase in $[Ca^{2+}]_i$: (1) increase in Ca^{2+} influx at each stimulus, (2) decrease in Ca^{2+} removal rate from the terminal cytoplasmic space, and (3) increase in Ca^{2+} outflow rate from the organelles into the cytosol. These possibilities will be examined in the next section.

A small decline of the $[Ca^{2+}]_i$ was seen at 13 and 33 Hz stimulation within the first 10 s after start of stimulation. The decline was also observed in three other terminals at 10–33 Hz stimulation. This may be due to a slow decrease of stimulation-induced Ca^{2+} influx from the external and/or increase in Ca^{2+} removal rate (see Discussion).

The value of the power index, *n*, obtained by the relationship between the $\Delta[Ca^{2+}]_i$ at the 80th to 100th stimuli ($\Delta[Ca^{2+}]_{p80-100}$: the same as $\Delta[Ca^{2+}]_{pl}$ in the short-term stimulation) and the stimulation frequency (cf. Eq. 9 and Fig. 3) was 1.87 in this figure and 2.03 ± 0.09 ($N = 4$) on the average. These are in good agreement with those obtained at the short-term stimulation (Table 1). The values of *n* obtained by the $\Delta[Ca^{2+}]_i$ 10 s after the start of stimulation (the average of $\Delta[Ca^{2+}]_i$ from 9 to 10 s after the start) and at the end of long-term stimulation (the average of $\Delta[Ca^{2+}]_i$ from 59 to 60 s after its start) were 1.79 ± 0.18 and 1.64 ± 0.04 ($N = 4$), respectively. They were a little smaller than those after 100 stimuli, due to gradual increase in the $\Delta[Ca^{2+}]_i$ at higher stimulation frequencies, but were obviously larger than unity, in contrast to the results of crayfish (Tank et al., 1995), suggesting existence of cooperativity in the Ca^{2+} removal system.

Decay time course of $\Delta[Ca^{2+}]_i$ after 60 s stimulation

The recovery process of $[Ca^{2+}]_i$ after stimulation for 60 s was strikingly different from that after short-term stimulation and was also obviously biphasic. As seen in Fig. 8 *A* and in the expanded time scale in Fig. 8 *B* (right), after the end of the 20–50 Hz stimulation $[Ca^{2+}]_i$ plunged sharply, first with a rate similar to that after short-term stimulation (cf. Figs. 3 *A*, 4), but with its decrease abruptly slowing a few seconds later. Thus, the recovery time course of $[Ca^{2+}]_i$ after high frequency stimulation consists of clearly separable rapid and slow decay phases.

The magnitude of the slow phase markedly increased with the stimulation frequency as shown in Fig. 8 *C*. Similar results were obtained in 3 other terminals ($N = 4$). The decay time constants, determined by fitting the slow phase of $[Ca^{2+}]_i$ recovery from 10 to 140 s after the stimulation with an exponential term, were 31 ± 9 s, 16 ± 3 s, 30 ± 9 s, and 67 ± 35 s after 13.3, 20, 33.3, and 50 Hz stimulation ($N = 4$), respectively. The larger amount of $[Ca^{2+}]_i$ decay at higher frequencies during slow recovery phase indicates that gradual $[Ca^{2+}]_i$ increase in the late phase during the long-term stimulation is difficult to explain solely by the gradual increase in Ca^{2+} inflow at each nerve stimulus (possibility 1). Instead, the slow recovery phase may be due

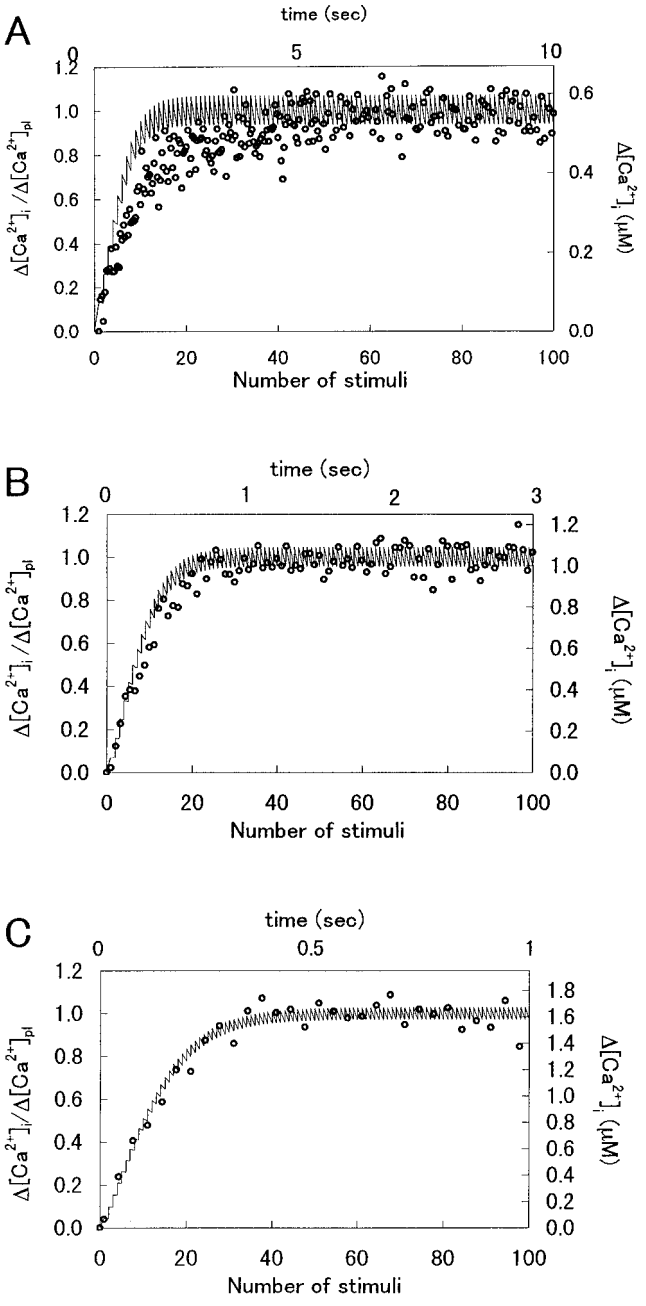

FIGURE 7 Time courses of $\Delta[Ca^{2+}]_i$ increases at a presynaptic terminal during short-term stimulation. The observed changes in $\Delta[Ca^{2+}]_i$ (*open circles*) and the simulated curves (*solid lines*) using the parameters, *n* and *k*, of the $\Delta[Ca^{2+}]_i$ decay time course after 100 stimuli are plotted against the number of stimuli at three stimulation frequencies: 10 Hz (*A*), 33.3 Hz (*B*), and 100 Hz (*C*). $\Delta[Ca^{2+}]_i$ is shown by the normalized values at the plateau (*left ordinate*) or by concentration (*right ordinate*). Elapsed times after start of stimulation are also shown in the upper abscissas. Concentration of OGB-2 was estimated to be about 110 μM (not overloaded).

to decrease of Ca^{2+} extrusion from the cytosol, increase of Ca^{2+} efflux from the organelles into the cytosol (possibilities 2 and 3), or both.

We also analyzed the rapid recovery phase for the period of 10 s after 60 s stimulation using Eq. 12 in the same way as in the short-term stimulation. Using the same *n* and *k* (1.87 and 2.44, respectively, in Fig. 8 *B*, *right*), all the recovery curves in a terminal at different stimulation frequencies were fitted well by changing only the values of *A* and *C*. The average value of *n* and *k* were 2.03 ± 0.09 and 2.56 ± 0.58 ($N = 4$), respectively. This was in fairly good agreement with the values of *n* and *k* estimated at these 4 terminals from the recovery process after the short-term 100 stimuli at various stimulation frequency, 1.94 ± 0.09 and 2.09 ± 0.53, respectively. Although *k* appeared to be increased about 20% by the long-term stimulation, this was not statistically significant ($p > 0.2$ by *t*-test).

These results suggest that the rapid recovery phase after long-term stimulation can be accounted for by the assumption that only the level of $[Ca^{2+}]_i$ at which the cooperative Ca^{2+} removal mechanism begins to work changes with stimulation, with little change in other parameters, i.e., *n* and *k*. In the analysis of short-term stimulation, we curve-fitted the recovery process after 100 stimuli using Eq. 12, in which we assumed that a constant and small *C* represents a very slow and additional decay process of $\Delta[Ca^{2+}]_i$. If the *C* is not negligible, the differential equation to obtain Eq. 12 is not Eq. 10 but is

$$\frac{d}{dt}(\Delta[Ca^{2+}]_i - C) = -k(\Delta[Ca^{2+}]_i - C)^n + f\delta_{CaF} \qquad (14)$$

where $\delta_{CaF} = 0$ after the stimulation. This equation means that the rate of Ca^{2+} removal is proportional to the square ($n = 2$) of the difference between cytoplasmic $[Ca^{2+}]_i$ and calcium concentration at somewhere, $([Ca^{2+}]_{rest} + C)$. Because the plateau value of $\Delta[Ca^{2+}]_i$ during stimulation is given as $(f\delta_{CaF}/k)^{1/n} + C$ (cf. Eq. A7 in Appendix 2), the slow phase increase in $[Ca^{2+}]_i$ during the long-term stimulation described above can be regarded as a gradual increase in *C*. The value of *C* decreased gradually after stimulation but was regarded as a constant within several seconds after the end of stimulation (Fig. 8, *A* and *B*). The results suggests that *C* represents the amount of calcium concentration accumulated in organelle. During long-term stimulation, Ca^{2+} removal by the organelle might decrease or Ca^{2+} efflux from the organelle into the cytosol increase because of Ca^{2+} accumulation in the organelle, or both (see Discussion). The values of *C* estimated in this way markedly increased with the stimulation frequency and were nearly equal to $\Delta[Ca^{2+}]_i$ at 10 s after the end of stimulation, as shown in Fig. 8 *C*. The whole time course of the slow phase after stimulation may be regarded as the recovery process of *C* to zero.

Relationship between the plateau values and the magnitudes of the slow decay phase after 60 s stimulation

Only the value of *C* is assumed to change during the long-term stimulation in the above interpretation. If this is correct, then the relation

$$\Delta[Ca^{2+}]_{p60s} - C_{60s} = \Delta[Ca^{2+}]_{p80-100} \qquad (15)$$

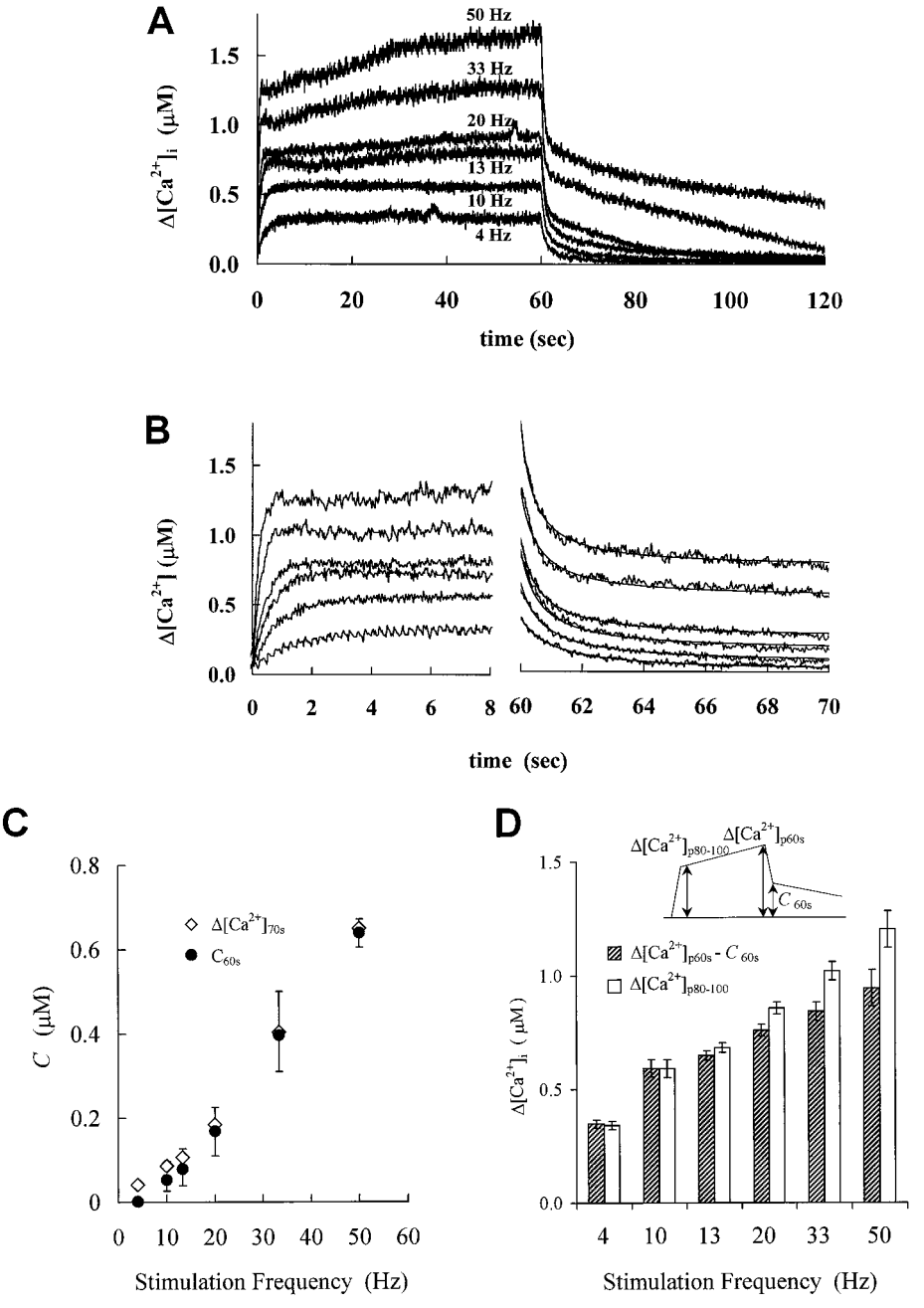

FIGURE 8 Changes in $\Delta[Ca^{2+}]_i$ in a presynaptic terminal at the long-term stimulation for 60 s. Estimated concentration of OGB-2 was about 500 μM. (*A*) Whole time courses of $\Delta[Ca^{2+}]_i$ changes during and after stimulation for 60 s at various stimulation frequencies. (*B*) *Left:* Rising phase of $\Delta[Ca^{2+}]_i$ after the start of stimulation in an expanded time scale. *Right:* Decays of $\Delta[Ca^{2+}]_i$ for 10 s after the end of stimulation at various stimulation frequencies in the expanded time scale. Solid smooth lines are the best-fit curves by Eq. 12, using the same values of n (1.87) and k (2.44). Values of $\{A, C\}$ are {0.35, 0.01}, {0.52, 0.07}, {0.70, 0.15}, {0.67, 0.23}, {0.76, 0.51}, and {0.97, 0.72} μM at 4, 10, 13.3, 20, 33.3, and 50 Hz stimulation, respectively. (*C*) Plot of the magnitudes of the slow decay component, C, against stimulation frequency. The values of C were estimated using Eq. 12 to fit a curve of the fast decay phase for 10 s after the end of stimulation (C_{60s}; *closed circles* − SE), or as the values of $\Delta[Ca^{2+}]_i$ 10 s after the end of stimulation ($\Delta[Ca^{2+}]_{70s}$: *open diamonds* + SE). The two agreed fairly well. (*D*) Comparison between $\Delta[Ca^{2+}]_{p60s} - C_{60s}$ (*shadowed bars* ± SE) and $\Delta[Ca^{2+}]_{p80-100}$ (*open bars* ± SE) in Eq. 15 due to long-term 60 s stimulation.

must hold (see Appendix 2), where $\Delta[Ca^{2+}]_{p60s}$ is the average of $\Delta[Ca^{2+}]_i$ during the last 1 s in the long-term stimulation, and C_{60s} is the value of C at the end of 60 s stimulation, estimated by fitting the decay time course of $\Delta[Ca^{2+}]_i$ for 10 s after 60 s stimulation with Eq. 12 (Fig. 8 *C*). Comparison between $(\Delta[Ca^{2+}]_{p60s} - C_{60s})$ and $\Delta[Ca^{2+}]_{p80-100}$ at various stimulation frequencies is given in Fig. 8 *D*. Both agreed fairly well at stimulation frequency lower than 20 Hz. However, at 33 and 50 Hz, $\Delta[Ca^{2+}]_{p80-100}$ was a little larger ($p < 0.05$ by t-test) than $(\Delta[Ca^{2+}]_{p60s} - C_{60s})$. This discrepancy may be due to increase in k or the gradual decrease of the amount of Ca^{2+} influx per impulse, δ_{CaF}, during the long-term stimulation (see Discussion). Taking into account this reasoning, the above assumption of the change only in C can account for both the gradual increase in the plateau $[Ca^{2+}]_i$ during stimulation and appearance of large slow decay phase after stimulation.

DISCUSSION

Cooperative Ca^{2+} removal obtained by two complementary methods

We examined the cooperativity of the Ca^{2+} removal system using two types of analysis: first by analyzing the relationship between the stimulation frequency and the $\Delta[Ca^{2+}]_i$

plateau and second by analyzing the kinetics of recovery of $[Ca^{2+}]_i$ to the resting level after stimulation. In the short-term stimulation protocol, almost the same n values, about 2, were obtained by both analyses, although they were based on different assumptions about the Ca^{2+} dynamics. Here, we examine the assumptions.

Constant Ca^{2+} inflow per action potential

In analysis of the $[Ca^{2+}]_i$ plateau during short-term stimulation, we assumed that the Ca^{2+} inflow per action potential did not vary with the stimulation frequency.

Openings of Ca^{2+}-activated K^+ channels (gK_{Ca} channels) by a high concentration of Ca^{2+} near opened Ca^{2+} channels have been reported to change the time course of presynaptic action potentials (Sivaramakrishnan, 1991). This may reduce the duration of the Ca^{2+} channel opening and reduce Ca^{2+} inflow at higher $[Ca^{2+}]_i$.

We used the intracellular microelectrode to measure action potentials at the presynaptic excitatory main axon near the branch to the terminals. The action potentials broadened a few percent after 100 stimuli at 50 and 100 Hz (data not shown). This result suggests that change in Ca^{2+} inflow due to activation of gK_{Ca} channels by increased $[Ca^{2+}]_i$ at high frequency stimulation may not be large enough to account for the markedly less-than-linear curve in Fig. 3 *B*. Further investigation is necessary on this point.

Some Ca^{2+} channels may have been inactivated after the plateau was reached, as suggested by a small decline in the plateau value observed in 13–33 Hz stimulation (Fig. 8 *A*). The decline at the end of 50 Hz stimuli for 60 s was estimated to be about 38%, from the ratio of $(\Delta[Ca^{2+}]_{p60s} - C_{60s})^2$ to $(\Delta[Ca^{2+}]_{p80-100})^2$ at 50 Hz (cf. Eq. 15 and Appendix 2), under the assumption that the discrepancy between them is due solely to gradual decline of Ca^{2+} influx per stimulus during the long-term stimulation. This corresponds to a 1.3% decrease at the end of 100 stimuli at 50 Hz, under the assumption of constant decline. Similar estimation at other stimulation frequencies (including 100 Hz) suggests that the decrease may be less than a few percent at the end of 100 stimuli, and may not significantly affect the estimated value of n.

Inactivation of Ca^{2+} channels before the plateau was reached at 100 and 50 Hz stimulation is unlikely, because with appreciable inactivation, the $[Ca^{2+}]_i$ in Fig. 7 *C* (100 Hz) should rise much faster than was calculated. However, the two coincided well. Therefore, a significant effect of frequency-dependent decrease in Ca^{2+} inflow on the estimation of n is improbable.

Constant Ca^{2+} binding ratio, β

In the recovery kinetics analysis, a constant value of the Ca^{2+} binding ratio, β, was assumed in Eq. 3. As we show in Appendix 1, this assumption holds if the dissociation constants for Ca^{2+} of both the endogenous and exogenous Ca^{2+} buffers are larger than $[Ca^{2+}]_i$ (Eq. A5) or if a low-affinity endogenous buffer is predominant (Eq. A6). Because the endogenous Ca^{2+} buffer is believed to have a large K_B (>10 μM) in most neurons or chromaffin cells (Xu et al., 1997), the former condition may be fulfilled in the case of OGB-2 loading, which has K_B of about 3 μM and plateau values <2 μM (Table 1). In the case of OGB-1, the latter condition may be fulfilled because the n value of about 2 was unchanged in the analysis of the decay time course, and the value of k ($= \gamma/(1 + \beta)$) was larger (Table 2). Thus, the assumption of constant β may hold at least approximately.

In conclusion, the power index, n, of about 2 obtained by the two different methods in the short-term stimulation strongly suggests the existence of true cooperative Ca^{2+} removal mechanisms. This was further supported by the results of the long-term stimulation.

Effect of inaccuracy of in vitro calibration

Because we do not know the constituents of the cytoplasm, the parameters K_B and $\Delta F_{max}/F$ in Eq. 1 obtained by in vitro calibration were not exact. However, the results obtained here were qualitatively invariable. We altered the K_B of OGB-2 (original value, 3.0 μM) from 1 to 6 μM. (A change in the resting level of $[Ca^{2+}]_i$ (original, 100 nM) from 300 to 50 nM, leaving K_B as 3.0 μM, gives the same effect on $\Delta[Ca^{2+}]_i$.) We also altered $\Delta F_{max}/F$ (original value, 7.2) from 5 to 10 and analyzed a data set obtained on a terminal which had a power index n of 2.2 obtained from the plateau level and 2.4 from the decay time course after 100 stimuli at 100 Hz. The value of n estimated from both analyses changed only slightly, i.e., the value obtained from the plateau level was between 1.8 and 2.4, and that from $[Ca^{2+}]_i$ decay time course was between 2.2 and 2.5. In contrast, both the value of $\delta Ca_{Tot}/\gamma$ (original, 0.035) and the rate constant of Ca^{2+} removal, k (original, 3.5), varied widely, from 0.001 to 0.2 in the former and from 1 to 28 in the latter. We conclude that the cooperative nature of the Ca^{2+} removal system obtained here is qualitatively invariable, even if the calibration curve may not be exact.

Comparison with the results of crayfish NMJ

Tank et al. (1995) showed (in their Figure 3) a completely proportional relationship between the plateau $\Delta[Ca^{2+}]_i$ and the stimulation frequency. This result was in sharp contrast to our obviously less-than-linear relationship (Fig. 3). What caused the difference?

Both crayfish and spiny lobster belong to *Reptantia* in *Decapoda* of *Crustacea*, so they may have essentially the same synaptic mechanisms at the NMJ. However, crayfish are adapted to fresh water and spiny lobster to seawater. When the decay time courses of $\Delta[Ca^{2+}]_i$ after 3–10 stimuli were fitted by two exponential terms, the major fast component had a decay time constant of about 5 s in crayfish, against 0.3–0.7 s at 17°C in spiny lobster (cf. Fig. 4). The

Ca^{2+} removal system of the spiny lobster may be more efficient than that of the crayfish. With the long-term stimulation protocol shown in Fig. 8, which adopted the same stimulation period (60 s) as Tank et al. (1995, their Figure 3), the relationship between the stimulation frequency of 4–50 Hz and the plateau $\Delta[Ca^{2+}]_i$ (including the origin) at the end of 60 s stimulation could be best fitted by Eq. 9 with a power index, n, of 1.64 ± 0.04. This was obviously different from the strictly proportional relationship obtained by Tank et al. (1995). This clearly shows that properties of Ca^{2+} removal systems can differ by species.

The dissociation constant and concentration of Ca^{2+} indicators loaded into the presynaptic terminal were also different in the two studies. These could cause the difference in the recovery kinetics of $[Ca^{2+}]_i$ after stimulation (Tank et al., 1995). In that work, the dissociation constant of loaded Ca^{2+} indicator, Fura-2, was 0.865 μM and its terminal concentration was about 700 μM (in their Figure 3). Because Ca^{2+} binding ratio of Fura-2 (about 800) was larger than that of the endogenous buffer (about 600), decay of $[Ca^{2+}]_i$ at higher $[Ca^{2+}]_i$ became faster. In this work, the dissociation constant of OGB-2 was 3.0 μM and its terminal concentration was 100–500 μM (Table 1). The Ca^{2+} binding ratio of loaded OGB-2 was 30–170 (cf. Appendix 1), far less than those in Tank et al. (1995). Moreover, the low-affinity endogenous Ca^{2+} buffer may be predominant (Ca^{2+} binding ratio may be several hundred, as in the crayfish NMJ), as suggested for OGB-1. Thus, the assumption of constant β may hold in our experiments, and the cooperative behavior of $\Delta[Ca^{2+}]_i$ decay after stimulation may not be due to saturation of Ca^{2+} buffers.

Possibility of other models

Multiple exponential

We did not describe the post-tetanic $[Ca^{2+}]_i$ decay time courses after short-term stimulation by multiple exponential terms because it is hard to explain the result of Fig. 3. The description of the $[Ca^{2+}]_i$ decay time course by multiple exponential terms (Connor et al., 1986; Helmchen et al., 1996) implicitly assumes the existence of Ca^{2+} regulation systems that depend on factors other than $[Ca^{2+}]_i$ in a single compartment (see discussion of complex mechanisms below) or the existence of multiple compartments in the terminal (Kijima and Kijima, 1997). Intracellular organelles may be constituents of the multiple compartments. However, in the time range and stimulation numbers adopted for the short-term stimulation protocol, Ca^{2+} efflux from the organelles into cytosol may be negligible, because they may not be saturated with Ca^{2+}. Thus, the terminal cytoplasmic space can well be regarded as a single compartment.

Complex mechanisms

The single compartment model may hold approximately, but the deviation of the $[Ca^{2+}]_i$ decay time course from a single exponential may be accounted for by other complex mechanisms. In a recent study of the presynaptic terminals of cerebellar parallel fibers, the Ca^{2+} removal mechanism was well accounted for by the interplay between $[Ca^{2+}]_i$ and $[Na^+]_i$, which affects Na^+/Ca^{2+} exchange (Regehr, 1997). This mechanism may play a role at low $[Ca^{2+}]_i$ in the spiny lobster NMJ and may contribute to the change of n value dependent on number of stimuli.

Extension of our model

As we found that the value of n did not significantly exceed 2, we can propose an extension of our model and assume that there are two Ca^{2+} removal systems. One is a second-order cooperative calcium clearance system and the other is a linear system. The differential equation after the end of stimulation is written as

$$\frac{d}{dt}(\Delta[Ca^{2+}]_i) = -k_2(\Delta[Ca^{2+}]_i)^2 - k_1(\Delta[Ca^{2+}]_i) - k_0 \quad (16)$$

where k_0, k_1, and k_2 are the rate constants of free calcium extrusion. Both Ca^{2+} removal systems work in parallel at the single compartment of terminal cytoplasm. We tried to analyze the $[Ca^{2+}]_i$ decay after 10 and 100 stimuli at 50 Hz based on this model and obtained results satisfactory to fit the time course of $[Ca^{2+}]_i$ decay to a curve. The increase in n from 1.4 to 2 in Eq. 12 corresponded to a decrease in k_1 and an increase in k_2 in Eq. 16. At 50 Hz stimulation, values of $\{k_2, k_1, k_0\}$ were $\{2.0 \pm 0.3\ \mu M^{-1}\ s^{-1}, 0.9 \pm 0.2\ s^{-1}, -0.013 \pm 0.006\ \mu M\ s^{-1}\}$ after 10 stimuli, and $\{2.7 \pm 0.4\ \mu M^{-1}\ s^{-1}, -0.26 \pm 0.14\ s^{-1}, 0.013 \pm 0.008\ \mu M\ s^{-1}\}$ after 100 stimuli, respectively ($N = 8$). This indicates a remarkable increase in k_2 and reduction of k_1 after 100 stimuli compared to those after 10 stimuli. As described below, the increase in k_2 may correspond to activation of mitochondrial Ca^{2+} uptake, while the decrease in k_1 may correspond to an effect of accumulated Na^{2+} on the Na^+/Ca^{2+} exchanger and/or effects of other unknown mechanisms.

What is a Ca^{2+} clearance mechanism with the power index $n = 2$?

Our results suggested that the Ca^{2+} removal system contains a cooperative mechanism with Hill's coefficient of about 2. What mechanism performs this part? We think one of the most probable candidates is mitochondria. Mitochondrial Ca^{2+} uptake follows a second-order Hill equation (Gunter et al., 1994; Xu et al., 1997). Mitochondria are also known to play a dominant role in the clearance of large Ca^{2+} loads from cytosol (Nicholls and Åkermann, 1982; Herrington et al., 1996). In recent studies, mitochondria were also shown to play an important role in presynaptic Ca^{2+} regulation associated with tetanic stimulation (Babcock and Hille, 1997). Because the dissociation constant of mitochondrial uniporter for Ca^{2+} is >10 μM (Bygrave et al., 1971; Scarpa and Graziotti, 1973; Xu et al., 1997), our

low concentration approximation by Eq. 5 holds, if it plays a dominant role. In nerve terminals, mitochondria may play an important role at a concentration of only a few μM (David et al., 1998). At crayfish NMJ, several inhibitors of mitochondrial Ca^{2+} uptake and release blocked the persistence of presynaptic residual $[Ca^{2+}]_i$ (Tang and Zucker, 1997).

We showed that the recovery time course of $[Ca^{2+}]_i$ after long-term stimulation at stimulation frequencies higher than 20 Hz was clearly separated into rapid and slow recovery phases, and that the slow one became larger with increased stimulation frequency (Fig. 8). This slow phase is difficult to explain without taking into account the intracellular organelles (see below). To determine whether the candidate is mitochondria or not, pharmacological experiments will be necessary.

Changes in properties of Ca^{2+} removal system during long-term stimulation

The $\Delta[Ca^{2+}]_i$ plateau gradually increased during long-term stimulation and a large-magnitude slow decay phase appeared after the stimulation (Fig. 8). The slow decay phase is probably caused by Ca^{2+} accumulated in the terminal organelle during stimulation, because it is difficult to explain by change in the properties of Ca^{2+} extrusion systems located on the terminal plasma membrane. The slow phase may be caused by changes in the rate of Ca^{2+} removal into the intracellular organelle and/or Ca^{2+} efflux from the organelle. We showed in Results (cf. Fig. 8) that changes in both the plateau and decay of $\Delta[Ca^{2+}]_i$ can be accounted for by a model in which the level of $\Delta[Ca^{2+}]_i$ at which the cooperative Ca^{2+} removal system of the organelle begins to work (expressed by C) increases with stimulation, with little change in the parameters n and k. This means that net efflux from the organelle, i.e., the sum of the decrease in Ca^{2+} uptake from the cytosol and the increase in Ca^{2+} extrusion into the cytosol by the organelle, increases with long-term stimulation by the amount:

$$k(\Delta[Ca^{2+}]_i - C)^2 - k(\Delta[Ca^{2+}]_i)^2 = kC(2\Delta[Ca^{2+}]_i - C)$$

(cf. Eq. 14). It is difficult to determine whether decrease in uptake or increase in efflux is the major part of the change. However, the Ca^{2+} extrusion rate from the organelle into the cytosol must increase, because Ca^{2+} stored by the organelle must be removed within the period after stimulation during which $[Ca^{2+}]_i$ returns to the resting level.

CONCLUSION

The overall mechanisms of Ca^{2+} regulation at the spiny lobster motor nerve terminal suggested by this study are illustrated schematically in Fig. 9.

After brief stimuli (10 stimuli, Fig. 9 *A*), both the Ca^{2+} removal system proportional to $(\Delta[Ca^{2+}]_i)^2$ (mitochondria) and that proportional to $\Delta[Ca^{2+}]_i$ (Na^+/Ca^{2+} exchanger and

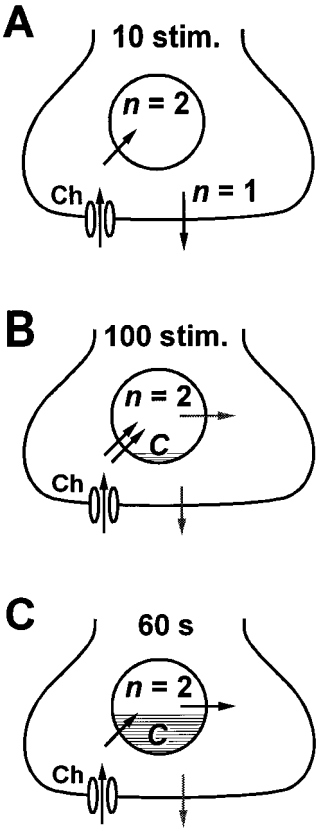

FIGURE 9 Schematic illustration of changes in Ca^{2+} dynamics dependent on the number or length of stimuli at the spiny lobster presynaptic terminal. Large circle shows the mitochondrion. Black double arrows, a black arrow, and a gray arrow show strong, medium, and weak flows of Ca^{2+}, respectively. Ch shows Ca^{2+} channels and C is Ca^{2+} accumulated in the mitochondrion. (*A*) During and after a brief stimulation (10 stimuli). (*B*) Just before and after the end of 100 stimuli. (*C*) Before and after the end of 60 s of stimulation at 20–50 Hz. See text for details.

Ca^{2+} pump) may work nearly equally. The value of n becomes about 1.5.

After 100 stimuli (Fig. 9 *B*), Ca^{2+} removal by the mitochondria may become predominant, probably due to activation of the mitochondrial uptake system and decrease in the Ca^{2+} removal efficiency of the Na^+/Ca^{2+} exchanger. The value of n becomes about 2 and a small effect of Ca^{2+} accumulation in the mitochondria (expressed by C) appears.

After 60 s stimulation (Fig. 9 *C*), Ca^{2+} removal by the mitochondria may be still predominant, but the effect of Ca^{2+} accumulation in the mitochondria becomes very large. The Ca^{2+} plateau gradually increases during stimulation due to increase in C and a large-magnitude slow decay phase appears.

APPENDIX 1

Ca^{2+} binding ratio, β

We defined the Ca^{2+} binding ratio, β, in Eq. 3 as a constant value. Here we describe it more precisely. Suppose there are an endogenous Ca^{2+} buffer,

S, and an exogenously added Ca^{2+} buffer or Ca^{2+} indicator, B (Neher, 1995). The total calcium concentration $[Ca^{2+}]_{Tot}$ is described as

$$[Ca^{2+}]_{Tot} = [Ca^{2+}]_i + [BCa] + [SCa] \quad (A1)$$

with

$$[BCa] = \frac{[B]_{Tot}[Ca^{2+}]_i}{[Ca^{2+}]_i + K_B} \quad \text{and} \quad [SCa] = \frac{[S]_{Tot}[Ca^{2+}]_i}{[Ca^{2+}]_i + K_S} \quad (A2)$$

where $[B]_{Tot}$ and $[S]_{Tot}$ are total concentrations of exogenous and endogenous buffer and K_B and K_S are their dissociation constants, respectively. The differential of $[Ca^{2+}]_{Tot}$ is given as:

$$\frac{d}{dt}[Ca^{2+}]_{Tot} = (1 + \beta)\frac{d[Ca^{2+}]_i}{dt} \quad (A3)$$

with

$$\beta \equiv \frac{\partial[BCa]}{\partial[Ca^{2+}]_i} + \frac{\partial[SCa]}{\partial[Ca^{2+}]_i} \quad (A4)$$

As is given in Eq. A4, β depends in general on $[Ca^{2+}]_i$.

The assumption of constant value of β holds if the dissociation constants for Ca^{2+} of both the endogenous and exogenous Ca^{2+} buffers are larger than $[Ca^{2+}]_i$, ($[Ca^{2+}]_i \ll K_B, K_S$), that is:

$$\beta \approx \frac{[B]_{Tot}}{K_B} + \frac{[S]_{Tot}}{K_S} = \text{constant} \quad (A5)$$

This also holds if a low-affinity endogenous buffer is predominant, even if the exogenous buffer has high affinity ($[B]_{Tot} \ll [S]_{Tot}$, $[Ca^{2+}]_i \sim K_B < K_S$).

$$\beta \approx \frac{[S]_{Tot}}{K_S} = \text{constant} \quad (A6)$$

Under these conditions, the value of β is constant and the definitions in Eq. 3 and Eqs. A3 and A4 are equivalent.

APPENDIX 2

Derivation of Equation 15

At the quasi-plateau, the left side of Eq. 14 is zero, that is:

$$\Delta[Ca^{2+}]_i - C = \left(\frac{f\delta_{CaF}}{k}\right)^{1/n} \quad (A7)$$

The right side of Eq. A7 is invariant during stimulation if the parameters of Ca^{2+} removal, n and k, are assumed to be unchanged. Eq. 15 then holds because the value of C after the 80th stimulus is negligibly small, as shown in the analyses of the short-term stimulation protocol (Tables 1 and 2).

REFERENCES

Abe, T., N. Kawai, and A. Miwa. 1983. Effects of a spider toxin on the glutaminergic synapse of lobster muscle. *J. Physiol.* 339:243–252.

Atluri, P. P., and W. G. Regehr. 1996. Determinants of the time course of facilitation at the granule cell to Purkinje cell synapse. *J. Neurosci.* 16:5661–5671.

Babcock, D. F., and B. Hille. 1998. Mitochondrial oversight of cellular Ca^{2+} signaling. *Curr. Opin. Neurobiol.* 8:398–404.

Baker, A. J., R. Brandes, J. H. M. Schreur, S. A. Camacho, and M. W. Weiner. 1994. Protein and acidosis alter calcium-binding and fluorescence spectra of the calcium indicator Indo-1. *Biophys. J.* 67: 1646–1654.

Bygrave, F. L., K. C. Reed, and T. Spencer. 1971. Cooperative interactions in energy-dependent accumulation of Ca^{2+} by isolated rat liver mitochondria. *Nature New Biol.* 230:89.

Carafoli, E., E. Garcia-Martin, and D. Guerini. 1996. The plasma membrane calcium pump: recent developments and future perspective. *Experientia.* 52:1091–100.

Connor, J. A., R. Kretz, and E. Shapiro. 1986. Calcium levels measured in a presynaptic neuron of *Aplysia* under conditions that modulate transmitter release. *J. Physiol.* 375:625–642.

David, G., J. N. Barrett, and E. F. Barrett. 1998. Evidence that mitochondria buffer physiological Ca^{2+} loads in lizard motor nerve terminals. *J. Physiol.* 509:59–65.

Delaney, K. R., and D. W. Tank. 1994. A quantitative measurement of the dependence of short-term synaptic enhancement on presynaptic residual calcium. *J. Neurosci.* 14:5885–5902.

Delaney, K. R., R. S. Zucker, and D. W. Tank. 1989. Calcium in motor nerve terminals associated with posttetanic potentiation. *J. Neurosci.* 9:3558–3567.

Dodge, F. A. Jr., and R. Rahamimoff. 1967. Co-operative action of calcium ions in transmitter release at the neuromuscular junction. *J. Physiol.* 193:419–432.

Fujii, J. T., F. T. Su, D. J. Woodbury, M. Kurpakus, X. J. Hu, and R. Pourcho. 1996. Plasma membrane calcium ATPase in synaptic terminals of chick Edinger-Westphal neurons. *Brain Res.* 734:193–202.

Galli, A., A. Ferroni, L. Bertollini, and M. Mazzanti. 1994. Inactivation of single Ca^{2+} channels in rat sensory neurons by extracellular Ca^{2+}. *J. Physiol.* 477:15–26.

Grynkiewicz, G., M. Poenie, and R. Y. Tsien. 1985. A new generation of Ca^{2+} indicators with greatly improved fluorescence properties. *J. Biol. Chem.* 260:3440–3450.

Gunter, T. E., K. K. Gunter, S. S. Sheu, and C. E. Gavin. 1994. Mitochondrial calcium transport: physiological and pathological relevance. *Am. J. Physiol.* 267:C313–C339.

Helmchen, F., K. Imoto, and B. Sakmann. 1996. Ca^{2+} buffering and action potential-evoked Ca^{2+} signaling in dendrites of pyramidal neurons. *Biophys. J.* 70:1069–1081.

Helmchen, F., J. G. Borst, and B. Sakmann. 1997. Calcium dynamics associated with a single action potential in a CNS presynaptic terminal. *Biophys. J.* 72:1458–1471.

Herrington, J., Y. B. Park, D. F. Babcock, and B. Hille. 1996. Dominant role of mitochondria in clearance of large Ca^{2+} loads from rat adrenal chromaffin cells. *Neuron.* 16:219–228.

Hua, S.-Y., M. Nohmi, and K. Kuba. 1993. Characteristics of Ca^{2+} release induced by Ca^{2+} influx in cultured bullfrog sympathetic neurons. *J. Physiol.* 464:245–272.

Iino, M., M. Koike, T. Isa, and S. Ozawa. 1996. Voltage-dependent blockage of Ca^{2+}-permeable AMPA receptors by joro spider toxin in cultured rat hippocampal neurones. *J. Physiol.* 496:431–437.

Jaffe, D. B., D. Johnston, N. Lasser-Ross, J. E. Lisman, H. Miyakawa, and W. N. Ross. 1992. The spread of Na^+ spikes determines the pattern of dendritic Ca^{2+} entry into hippocampal neurons. *Nature.* 357:244–246.

Kamiya, H., and R. S. Zucker. 1994. Residual Ca^{2+} and short-term synaptic plasticity. *Nature.* 371:603–606.

Katz, B., and R. Miledi. 1968. The role of calcium in neuromuscular facilitation. *J. Physiol.* 195:481–492.

Kawai, N., A. Mauro, and H. Grundfest. 1972. Effect of black widow spider venom on the lobster neuromuscular junction. *J. Gen. Physiol.* 60:650–664.

Kijima, H., and S. Kijima. 1997. Theoretical approaches to ion channel dynamics and the first-order reaction. *In* Progress in Cell Research, vol. 6. M. Sokabe, A. Auerbach, and F. Sigworth, editors. Elsevier, Amsterdam. 295–304.

Konishi, M., A. Olson, S. Hollingworth, and S. M. Baylor. 1988. Myoplasmic binding of fura-2 investigated by steady-state fluorescence and absorbance measurements. *Biophys. J.* 54:1089–1104.

Llinás, R., M. Sugimori, and R. B. Silver. 1992. Microdomains of high calcium concentration in a presynaptic terminal. *Science.* 256:677–679.

Luther, P. W., R. K. Yip, R. J. Bloch, A. Ambesi, G. E. Lindenmayer, and M. P. Blaustein. 1992. Presynaptic localization of sodium/calcium exchangers in neuromuscular preparations. *J. Neurosci.* 12:4898–4904.

Lytton, J., M. Westlin, S. E. Burk, G. E. Shull, and D. H. MacLennan. 1992. Functional comparisons between isoforms of the sarcoplasmic or endoplasmic reticulum family of calcium pumps. *J. Biol. Chem.* 267: 14483–14489.

Magleby, K. L., and J. E. Zengel. 1982. A quantitative description of stimulation-induced changes in transmitter release at the frog neuromuscular junction. *J. Gen. Physiol.* 80:613–638.

Mullins, L. J. 1977. A mechanism for sodium/calcium transport. *J. Gen. Physiol.* 70:681–695.

Neher, E. 1995. The use of Fura-2 for estimating Ca buffers and Ca fluxes. *Neuropharmacology.* 34:1423–1442.

Neher, E., and G. J. Augustine. 1992. Calcium gradients and buffers in bovine chromaffin cells. *J. Physiol.* 450:273–301.

Nicholls, D., and K. Åkerman. 1982. Mitochondrial calcium transport. *Biochem. Biophys. Acta.* 683:57–88.

Ravin, R., M. E. Spira, H. Parnas, and I. Parnas. 1997. Simultaneous measurement of intracellular Ca^{2+} and asynchronous transmitter release from the same crayfish bouton. *J. Physiol.* 501:251–262.

Regehr, W. G. 1997. Interplay between sodium and calcium dynamics in granule cell presynaptic terminals. *Biophys. J.* 73:2476–2488.

Regehr, W. G., and P. P. Atluri. 1995. Calcium transients in cerebellar granule cell presynaptic terminals. *Biophys. J.* 68:2156–2170.

Sala, F., and A. Hernández-Cruz. 1990. Calcium diffusion modeling in a spherical neuron: relevance of buffering properties. *Biophys. J.* 57: 313–324.

Scarpa, A., and P. Graziotti. 1973. Mechanisms for intracellular calcium regulation in heart. I. Stopped-flow measurements of Ca^{2+} uptake by cardiac mitochondria. *J. Gen. Physiol.* 62:756–772.

Shudo, K., Y. Endo, Y. Hashimoto, Y. Aramaki, T. Nakajima, and N. Kawai. 1987. Newly synthesized analogues of the spider toxin block the crustacean glutamate receptor. *Neurosci. Res.* 5:82–85.

Sivaramakrishnan, S., G. D. Bittner, and M. S. Brodwick. 1991. Calcium-activated potassium conductance in presynaptic terminals at the crayfish neuromuscular junction. *J. Gen. Physiol.* 98:1161–1179.

Tanabe, N., and H. Kijima. 1992. Ca^{2+}-dependent and -independent components of transmitter release at the frog neuromuscular junction. *J. Physiol.* 455:271–289.

Tang, Y., and R. S. Zucker. 1997. Mitochondrial involvement in post-tetanic potentiation of synaptic transmission. *Neuron.* 18:483–491.

Tank, D. W., W. G. Regehr, and K. R. Delaney. 1995. A quantitative analysis of presynaptic calcium dynamics that contribute to short-term enhancement. *J. Neurosci.* 15:7940–7952.

Walrond, J. P., C. K. Govind, and S. E. Huestis. 1993. Two structural adaptations for regulating transmitter release at lobster neuromuscular synapses. *J. Neurosci.* 13:4831–4845.

Xu, T., M. Naraghi, H. Kang, and E. Neher. 1997. Kinetic studies of Ca^{2+} binding and Ca^{2+} clearance in the cytosol of adrenal chromaffin cells. *Biophys. J.* 73:532–545.

Zucker, R. S. 1996. Exocytosis: A molecular and physiological perspective. *Neuron.* 17:1049–1055.